Explorative Study on a Discrete Particle Model for Sheet Flow Simulations

Renske Gelderloos

January 2008

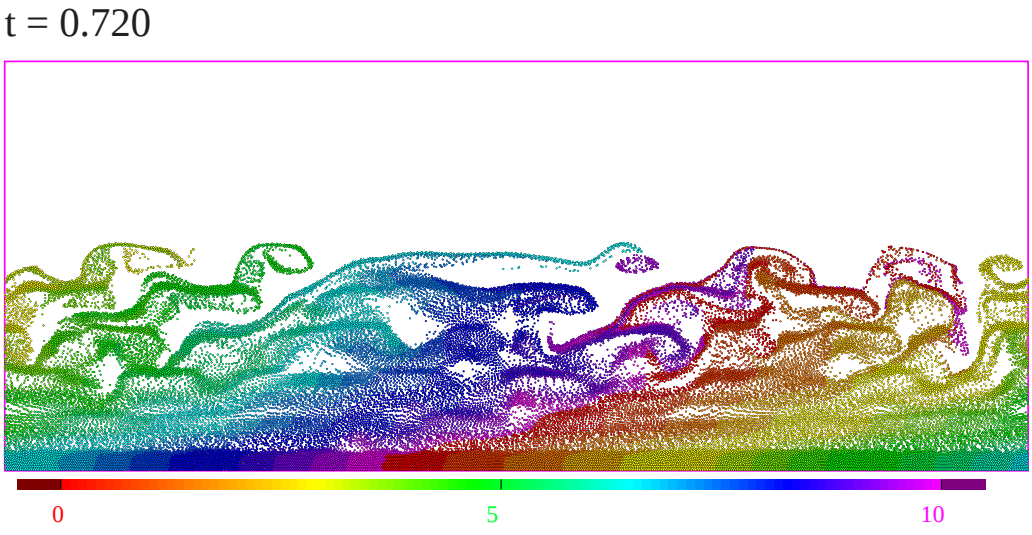

Explorative Study on a Discrete Particle Model for Sheet Flow Simulations

MSc. Thesis

Renske Gelderloos

University of Twente
Department of Civil Engineering

Graduation committee:

Prof. dr. S.J.M.H. Hulscher

Dr. ir. J. S. Ribberink

Dr. ir. M.A. van der Hoef

Prof. dr. ir. J.A.M. Kuipers

January, 2008

Abstract

Under high waves in shallow water a high energy sediment transport regime occurs called 'sheet flow'. In this regime large amounts of sediment are transported in a short time interval. Reliable prediction methods for this transport regime are therefore very important to civil engineers. However, mainly due to lack of insight in the underlying physical phenomena predictive models still fail too often.

In this study a relatively new approach was followed in order to increase the understanding of sheet flow. A very detailed computer model was used to simulate sheet flow up to the level of individual sand particles (a Discrete Particle Model, DPM). Although we did not succeed in making simulations of actual sheet flow cases, this explorative study shows that the potential value of DPM simulations for sediment transport is substantial as many issues of uncertainty in existing models can be studied in detail using a DPM. This report will give an overview of the possibilities as well as the limitations of DPM-simulations for sheet flow modelling.

List of symbols

Symbol	Description	Unit
A_p	Projected area of a sediment particle	
a_x	Acceleration associated with the horizontal body forcing representing the fluid pressure	$\mathrm{m/s^2}$
C	Volumetric sediment concentration	$\mathrm{m^3/m^3}$
C_0	Maximum sediment concentration	$\mathrm{m^3/m^3}$
C_D	Drag coefficient	
C_L	Lift coefficient	
C_M	Added mass coefficient	
D	Particle diameter	m
D_{50}	Median particle diameter	m
d_c	Erosion depth	m
e	Coefficient of normal restitution	
e_t	Coefficient of tangential restitution	
f	Interaction force between fluid and particle phase	N
$\mathbf{F}$	Force	N

Symbol	Description	Unit
g	Acceleration due to gravity	m/s^2
$\mathbf{I}$	Unit tensor	
I	Moment of inertia	
k_n	Linear spring stiffness	N/m
k_s	Roughness height	m
k_t	Tangential spring stiffness	N/m
m_a	Mass of particle a	kg
p	Fluid pressure	N/m^2
$\mathbf{r}$	Position vector	[m,m,m]
$\mathbf{r}_a$	Position vector of particle a	[m,m,m]
R_a	Radius of particle a	m
Re_p	Reynolds particle number	
$\vec{\mathbf{S}}_P$	Source term representing momentum exchange from solid phase to fluid phase	N/m^3
t	Time	s
$\mathbf{T}$	Torque	Nm
$\mathbf{u}$	Flow velocity	m/s
$\mathbf{v}_a$	Velocity of particle a	m/s
u_j	Flow velocity in the j-direction	m/s
U_w	Free stream velocity	m/s
V	Total volume	m^3
V_a	Volume of particle a	m^3
V_p	Particle volume	m^3

Symbol	Description	Unit
(x, y, z)	Cartesian coordinates	[m,m,m]
β	momentum transfer coefficient	
$\delta(...)$	Delta function	
δ_{ij}	Kronecker Delta	
δ_s	Sheet flow layer thickness	m
ϵ	Local porosity	
ρ	Water density	kg/m^3
ρ_s	Sediment density	kg/m^3
η_n	Normal damping coefficient	Ns/m
η_t	Tangential damping coefficient	Ns/m
θ	Shields parameter	
θ_{cr}	Critical value of Shields parameter	
λ	Dilatational viscosity of a fluid	Pa.s
μ	Molecular viscosity of water	Pa.s
μ_f	Friction coefficient for particle collisions	
$\vec{\tau}$	Viscous stress tensor	N/m^2
τ_b	Bed shear stress	N/m^2
ϕ	Dynamic friction angle of sediment	degrees
ω_a	Angular velocity of particle a	s^{-1}

Preface

Looking for a project for my masters thesis I came across a somewhat vague description of an opportunity to try and use a model used in chemical engineering for civil engineering purposes. The project looked like a challenge, not least because it had already been available for two years. And a challenge it turned out to be. Besides learning a new programming language and learning to work in Linux, I also learned much more about CFD as well as sediment transport. But perhaps the biggest challenge was to communicate with both chemical engineers and civil engineers, as their technical jargon and scientific approach is hardly even closely resembling. Nevertheless I have tried my best to make this report well readable for both groups.

I think this personal note in my masters thesis is a nice place to thank some people, without who I would never have come this far. First of all I would like to thank my graduation committee prof. dr. Suzanne Hulscher, dr. ir. Jan Ribberink, dr. ir. Martin van der Hoef, and prof. dr. ir. Hans Kuipers for their input and enthusiasm, and for giving me all the space I needed to go and explore by myself. Furthermore I would like to thank the Fundamentals of Chemical Reaction Engineering group for their completely disinterested help in providing a place to work and a large stack of knowledge and experience in CFD from which I could make use anytime. I have felt very welcome from

the very first day. In particular I would like to thank ir. Willem Godlieb for all the help he has given me on getting to know the DPM and solving all the problems I encountered in working with the code during this project. Thank you all.

Renske Gelderloos

January 2008

Contents

Chapter 1

Introduction

Reliable predictions of coastline evolution is of primary importance to civil engineering practice. Profound knowledge of the magnitude and direction of sediment transport in coastal areas is therefore essential. Under high waves in shallow water a high energy transport regime called sheet flow can occur. A whole layer of sediment is then set into motion, as a result of which very large sediment fluxes are observed. As one can imagine, the influence of the sediment transport under sheet flow conditions on coastal morphology can be relatively large.

The focus of the current research on sheet flow is mainly on experiments (e.g. [33], [23], [11], [28], [29]) and (mostly empirical) model predictions (e.g. [31], [8], [14]). In the empirical models often the assumption is made that the sediment movement adapts instantaneously to changes in the flow velocity. This is true if the phase-lag between the sediment concentration is small compared to the wave period. In steady flows the assumption of instantaneous response tends to hold, but especially in oscillatory flows the unsteady flow behaviour often makes the assumptions to break down [12]. Therefore, a need

is observed for models based on physical principals which can accurately account for unsteadiness and non-instantaneous responses of sediment transport to changes in flow velocity. However, about the complex sediment-water interaction mechanisms still very little is well understood. In this study, a first attempt is made to simulate the motion of individual sand particles under the influence of water motion, and the influence of the sand particles on the flow in return in order to increase the understanding of the underlying physical phenomena of sheet flow. The results of this study did not lead to a fully operational Discrete Particle Model (DPM), but merely give an idea of the potential value of a DPM for sheet flow predictions and discusses the difficulties to be taken into account in future research.

The aim of this study is go gain a better insight in the behaviour of the flow of water and sediment and their interaction in the case of sheet flow. Therefore a numerical computer model[1], usually employed for chemical engineering research purposes, was used to simulate in detail the water motion, the motion of individual sand particles and the interaction between the two phases. The following research questions are addressed in this report:

1. Which points of dispute in existing sheet flow models could be studied with the help of a DPM?

2. Can this DPM simulate horizontal sediment movement in water? If so, how does it perform for sheet flow?

In order to investigate whether and how a DPM could contribute to our understanding of sheet flow processes the following approach was followed.

[1]The Discrete Particle Model was provided by the Fundamentals of Chemical Reaction Engineering group of the Chemical Engineering department of the University of Twente.

First an overview of the presently existing sheet flow models was created by means of a literature review. The aim of this part of the study was to identify different types of models and point out their purpose and possibilities together with their advantages and disadvantages. By putting the DPM in this overview of model types, an idea was formed about the possibilities and limitations of the use of DPM's for sheet flow modelling.

Next a DPM was created that could be suitable for sheet flow simulations. The starting point was an existing DPM used for the simulation of chemical engineering processes, such as gas fluidisations. In order to be able to simulate the behaviour of sand moving horizontally over a sand bed under the influence of water, some adaptations were implemented in the model. Due to lack of time only the most crucial changes were made. This is however sufficient to get a first impression of the suitability of the DPM for sheet flow modelling. The model could run on computer clusters available at the university.

In chapter 2 the theory of sediment transport and in particular sheet flow will be discussed. Chapter 3 discusses conventional sheet flow modelling and advantages and disadvantages of different types of models. Chapter 4 comprises a comprehensive description of the DPM and the adaptations that where made in order to make the model suitable for the simulation of sediment transport. In chapter 5 the model results are given. In chapter 6 the results will be discussed and in chapter 7 conclusions are drawn and some recommendations for further research will be given.

Chapter 2

Theory

The interaction of water and sediment on the sea floor is a complex phenomenon. Therefore, some theoretical aspects of the hydrodynamics and particle dynamics, necessary for the understanding of sheet flow, will be dealt with first separately. Then the influence of the hydrodynamics on the particle dynamics are discussed in the section on sediment transport. Finally, some specific characteristics of sheet flow are discussed.

2.1 Hydrodynamics

2.1.1 Driving forces

A distinction should be made between sheet flow in steady uniform flow and oscillatory flow. In the case of unidirectional sheet flow gravity is the driving force behind the flow [22]. This sheet flow type is experimentally investigated in a tilted flume, as a result of which the gravitational force has a component along the flume bottom. In the case of oscillatory sheet flow, the driving force behind the flow is a (horizontal) pressure gradient [25]. Under shallow water

waves, the orbital motion of the water particles evolves from circular near the surface, to ellipses closer to the bottom and a merely to and fro motion very close to the bottom. Experimental research on oscillatory sheet flow is usually done in large scale oscillatory flow tunnels, in which a piston provides a pressure difference.

2.1.2 Boundary layer flow

The driving forces cause the water to flow. As the water flows over the bottom a boundary layer develops. In the case of unidirectional flow this boundary layer can be rather large, up to the whole water depth in case of rivers. In the case of oscillatory flow, predominant in near coast wave dominated environments, the boundary layer breaks up every half wave cycle and therefore does not get the chance to fully develop. The boundary layer thickness under waves is therefore rather small [10].

Boundary layer flow is important for sediment transport as inside the boundary layer the water is slowed down by the presence of the sea floor. A velocity profile develops, ranging from the free stream velocity on the top of the boundary layer to zero velocity at the bottom (no slip). Naturally, as the bed poses a shear stress on the water, the water flow poses a shear stress on the bed as well. This shear stress is called the bed shear stress (τ_b). The bed shear stress is one of the most important parameters in sediment transport as it causes the sediment to move.

2.2 Particle dynamics

2.2.1 Material properties

Dutch coastal sediment typically consists of mainly quartz sand, with a density of $\rho_s = 2650 kg/m^3$. The sediment contains a range of particle sizes. In this study we will constrain ourselves to uniform sand of $0.2mm$ in diameter. This is well beyond the cohesive limit of $0.062mm$, and in addition in the order of magnitude often used in experimental research. According to Dohmen-Janssen [10], the shape of the grains and the composition of the sediment are also relevant to sediment transport processes. These aspects are however not included in the model used in this study.

2.2.2 Forces on a particle

The balance of forces on an individual sand particle is formed by gravity, drag, and lift forces. The two latter are generated by water motion and can thus vary in time and space, while the former is related to the Earth's gravitational field and therefore only depends on the mass of the particle. Drag and lift are mobilising forces. Gravity is mostly a stabilising force, but on a sloping bed it has a mobilising influence as well. If the mobilising forces overtake the stabilising forces, the particle is set into motion. The relative importance of the mobilising and stabilising forces is given by the Shields parameter [10]:

$$\theta(t) = \frac{\tau_b(t)}{(\rho_s - \rho)\, gD} \tag{2.1}$$

where $\theta(t)$ is the non dimensional Shields parameter, τ_b is the bed shear stress, ρ_s is the density of the sediment, ρ is the water density, g is the gravitational

acceleration, and D is the particle diameter.

2.3 Sediment transport

If the Shields parameter exceeds a certain critical value (θ_{cr}), sediment is set into motion. For increasing values of θ the sediment load alters depending on the transport regime (figure 2.1). The following regimes are generally recognised [10]:

- No sediment transport ($\theta < \theta_{cr}$)
- Bed load regime
  - $\theta > \theta_{cr}$
  - particles are in almost continuous contact with the bed and each other, so intergranular forces are important
  - layer thickness in the order of a few grain diameters
- Bed load and suspended load regime
  - θ increased further
  - bed load and suspended load
  - ripples and/or dunes form on the bed
- Sheet flow
  - $\theta > 0.8 - 1.0$
  - ripples are washed out

– high sediment concentrations so grain-water interactions as well as intergranular forces are important

– bed load and suspended load

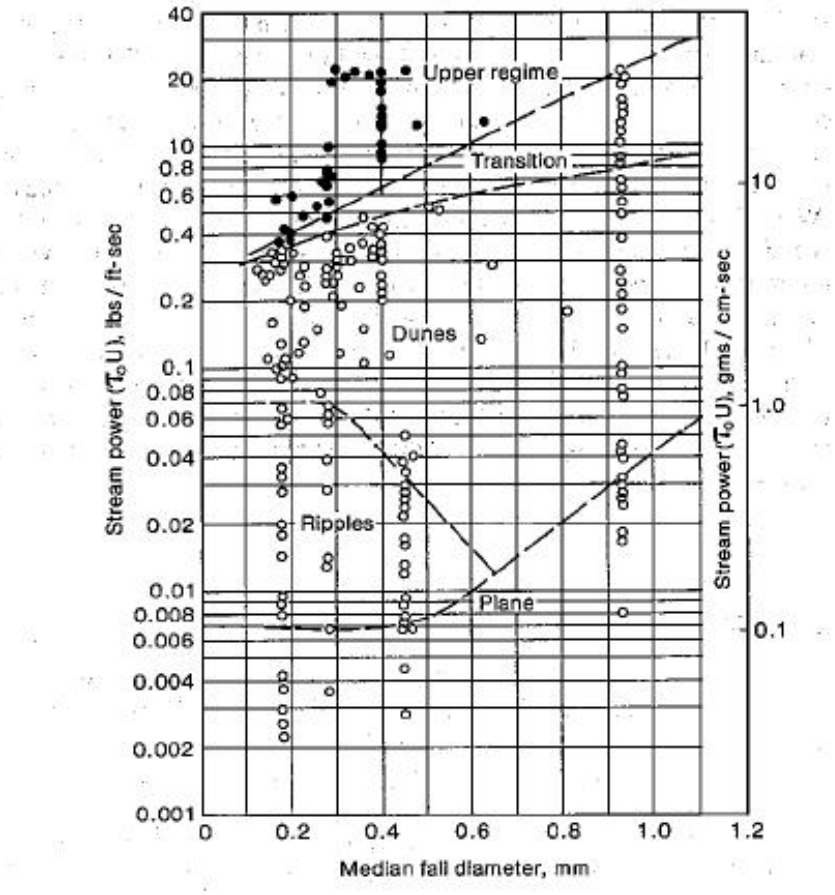

Figure 2.1: Sediment transport regimes. Sheet flow is situated in the upper left plane. Source: Chang [6]

2.4 Sheet flow characteristics

2.4.1 Composition of the sheet flow layer

The sheet flow layer can be divided into two layers [28]: the pick-up layer and the upper sheet flow layer (figure 2.2)[1]. In the pick-up layer sediment grains are picked up from the bed when the velocity over the bed increases. The sediment concentration therefore decreases in this layer when the flow accelerates. The sediment is transported upwards to the upper sheet flow layer where the sediment concentration subsequently increases. In oscillatory sheet flow the concentration profile in the upper sheet flow layer lags behind the concentration in the pick-up layer.

Two important parameters concerning the composition of the sheet flow layer appear in every text on sheet flow. First, the sheet flow layer thickness δ_s is the (vertical) distance between the bottom and upper limit of the sheet flow layer. On the bottom side, the sheet flow layer is bounded by the non moving bed. The upper side boundary is more arbitrary, mostly the level where a certain volume concentration occurs is chosen (for example the 8-volume percentage criterion by Dohmen-Janssen [10]). The erosion depth d_c is the distance between the still bed level at zero velocity and the still bed level at maximum velocity.

2.4.2 Time dependency: phase-lag effects

Two types of phase-lag effects are important in oscillatory sheet flow. First, the phase difference between the free stream flow and the flow velocity in the

[1]Figure based on figure in Dohmen-Janssen [10], p. 26.

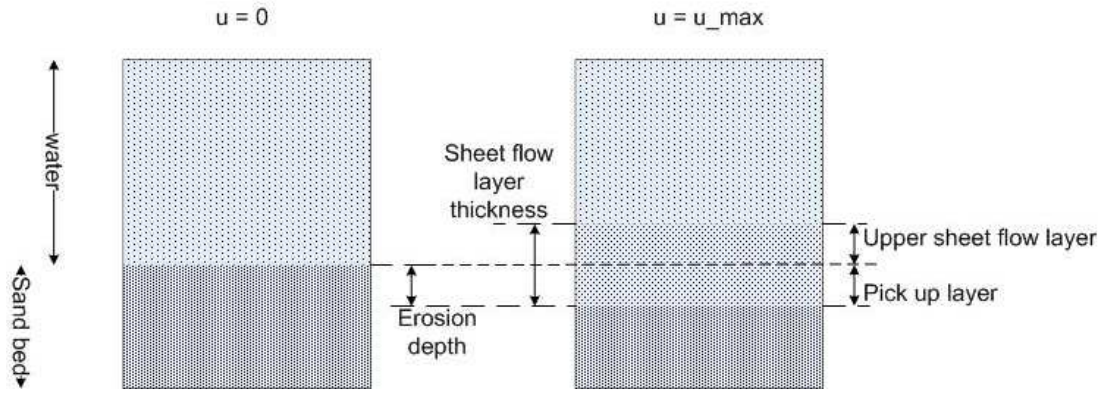

Figure 2.2: Composition of the sheet flow layer.

boundary layer in oscillatory flow. This is due to the inertia of the water itself. The water in the boundary layer contains less inertia and can therefore react more quickly to changes in the pressure gradient, giving the boundary layer flow a phase-lead with respect to the flow outside the boundary layer [10]. Second, the phase lag between the time dependent velocity profile and the time dependent concentration profile. This is because of three reasons: (1) it takes time for the grains to be picked up, (2) it takes time for the grains to be moved upwards and entrained into the flow, and (3) it takes time for the grain to settle again after the flow has decelerated. The size of this type of phase lag effect depends on the relative magnitude of the time needed for pick up and resettling with respect to the wave period.

2.4.3 Influence of the sediment on water (roughness height and turbulence damping)

The friction exerted by the bed on the flow can be parameterised by means of a roughness height k_s. The roughness height is a measure for the distance the disturbance protrudes into the flow. For a flat bed the median grain diameter D_{50} is mostly chosen as an appropriate value. However, experiments have shown that in case of sheet flow sediment transport the roughness height is better described by the sheet flow layer thickness δ_s [11].

In the sheet flow layer a very large concentration gradient exists. If the sand-water mixture is considered as a continuum, this would imply a large (negative) density gradient. Density gradients cause buoyancy forces as explained by Dohmen-Janssen [10], which in turn can cause a stable flow stratification. A stable flow stratification impedes the turbulent transport of mass and momentum, which is referred to as turbulence damping in sheet flow literature.

2.4.4 Influence of the water on the sediment (hindered settling)

A downward flux of sediment generally has to be compensated by an upward flux of water. In dilute systems this will only have a very small effect. However, because of the high concentration in a sheet flow layer the resettling grains can be hindered substantially by the 'up-flowing' water [10].

Chapter 3

Conventional sheet flow modelling

3.1 Model types

A variety of models can currently be found in literature for the calculation of sediment transport in sheet flow conditions. The three model types that can roughly be distinguished are summarised in figure 3.1.

The transport formulae give an empirical relation between the sediment flux and some physical parameters such as the average flow velocity, particle diameter, and sediment density. In the quasi-steady models (for example [3], [27], [39], [31]) the sediment transport is assumed to adopt instantaneously to (changes in) the flow velocity. This type of modelling is especially suitable for unidirectional flows and oscillatory flows in case phase lags are not significant. A big advantage of the quasi-steady model is that it provides a very quick estimate of the amount of sediment transport which makes it very suitable for engineering purposes. However, if the assumption of instantaneous

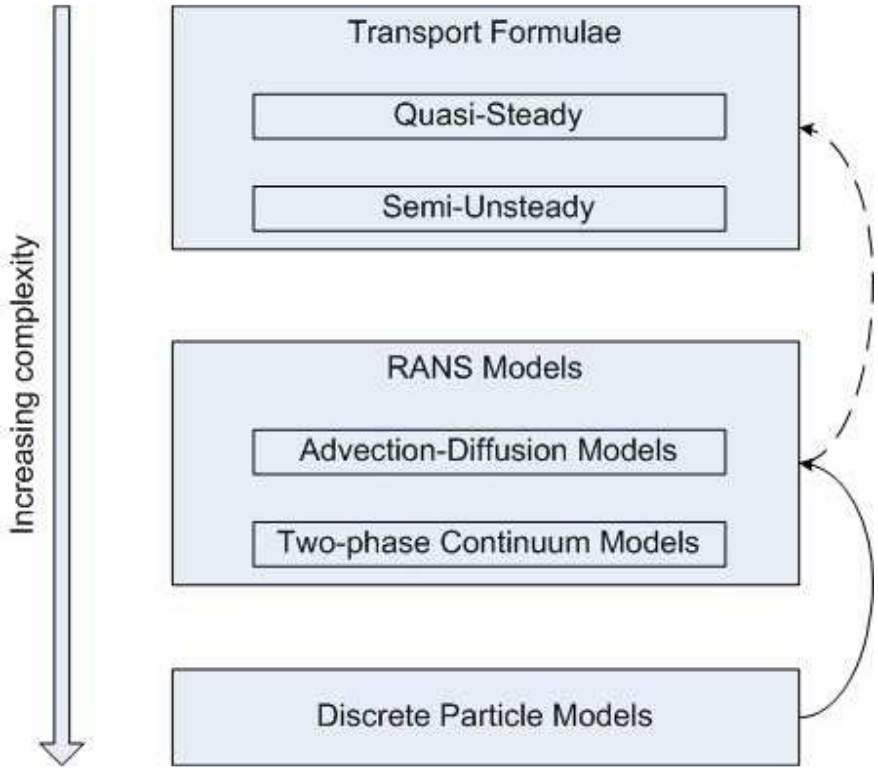

Figure 3.1: Sheet flow model types.

response to the flow breaks down, the model results are unreliable. Besides, the quasi-steady models are highly empirical and therefore give no insight in the underlying physics of the phenomenon. Sometimes the effect of phase lags are partially taken into account through parameterisations. This type of models is commonly referred to as semi-unsteady models (e.g. [9], [12]).

In the Reynolds Averaged Navier Stokes (RANS) models the movement of fluid and sediment are described separately. Both phases are treated as a continuum (Eulerian-Eulerian approach). In advection-diffusion models (e.g. [33], [8], [18]) the fluid dynamics are covered by a simple momentum equation where only flow in the x-direction is considered, and only the horizontal pressure gradient and turbulent diffusion are included as forces. The sediment concentration is often assumed low enough not to have a significant influence

on the fluid dynamics. In some models this influence is taken into account through a parametrisation of for example turbulence damping. The sediment dynamics are covered by an advection-diffusion equation for the sediment concentration. In the two-phase flow continuum models (e.g. [1], [14], [26]) the dynamics of the fluid and the sediment are both described by a mass and momentum balance where the mass and momentum balance for fluid act on the fluid fraction of the system and the mass and momentum balance for sediment on the sediment fraction. The two phases interact via drag, lift, and added mass. The exact description of these forces differs from one model to another. An advantage of the RANS models with respect to transport formulae is that the unsteady interaction between the fluid and solid phase can be accounted for. The more complex model description however requires more assumptions such as a suitable turbulence closure. The major advantage of the two-phase flow models over the advection-diffusion models is that they are better suitable for the modelling of the dynamics of a system with high sediment concentrations found in sheet flow.

The currently most refined models used for sediment transport modelling are the Discrete Particle Models ([37], [15], [17]). In these type of models the particles are not treated as a continuum but in a discrete way (Lagrangian approach). Interparticle interactions can therefore be taken into account explicitly. The fluid phase may either be modelled as a continuum or as discrete layers. A disadvantage of this model type is that it is severely limited by computational capacity of the computer, as a result of which simulations are limited to a small spatial and temporal extent. Furthermore, additional uncertainties are introduced in the values of new parameters (such as the simulation parameters in a particle collision model).

3.2 Relation between model types

As pointed out in figure 3.1, sheet flow models exist in different levels of complexity. Generally, the simplest models are mainly empirical, while the complex models contain a more physically based description of the phenomenon. So, the transport formulae are very useful to give a quick estimate of the net sediment transport. However, if the results turn out to be incorrect, it is hard to point out from a physical point of view what part of the model is wrong or incomplete. On the other hand, a DPM can by itself not simulate sheet flow processes on a useful scale for engineering purposes. However, the assumptions and simplifications made in larger scale models can be studied with the help of a DPM.

The solid arrow in figure 3.1 indicates that information from the DPM can be used in the RANS models. For example the relative importance of forces or the most appropriate choice of parametrisation of a certain turbulent quantity can be studied in detail with a DPM, and the results can be used in the continuum models. Some points of discussion which can be studied are given in the next section. The striped arrow in figure 3.1 indicates that information from continuum models can also be used to improve transport formulae. For example the importance and influence of unsteady effects can be studied with two phase continuum models, and the results can be used for the incorporation of unsteady effects in semi-unsteady transport formulae. This coupling is however outside the scope of this study, which focusses on DPM results.

3.3 Points of discussion

Here we will focus on the two-phase continuum models, as they are the closest to the DPM. A more elaborated overview of points of discussion in sheet flow models can be found in Appendix A.

For this study the models of Asano [1], Dong and Zhang [13] [14], and Liu and Sato [25] [26] where compared. The three models are all based on the following set of Reynolds-averaged equations:

$$\frac{\partial \rho\,(1-C)}{\partial t} + \frac{\partial \rho\,(1-C)\,u_j}{\partial x_j} = \frac{\partial \phi_j^m}{\partial x_j}$$

$$\frac{\partial \rho_s C}{\partial t} + \frac{\partial \rho_s C u_{s,j}}{\partial x_j} = \frac{\partial \phi_{s,j}^{s,m}}{\partial x_j}$$

$$\frac{\partial \rho\,(1-C)\,u_i}{\partial t} + \frac{\partial \rho\,(1-C)\,u_i u_j}{\partial x_j} = -\,(1-C)\,\frac{\partial p}{\partial x_i} - \rho\,(1-C)\,g\delta_{i2} + \frac{\partial \phi_i^a}{\partial t} + \frac{\partial \tau_{ij}^c}{\partial x_j} - f_i$$

$$\frac{\partial \rho_s C u_{s,i}}{\partial t} + \frac{\partial \rho_s C u_{s,i} u_{s,j}}{\partial x_j} = -C\frac{\partial p}{\partial x_i} - \rho_s C g \delta_{i2} + \frac{\partial \phi_{s,i}^{s,a}}{\partial t} + \frac{\partial \tau_{s,ij}^{s,c}}{\partial x_j} + \frac{\partial T_{s,ij}}{\partial x_j} + f_i$$

where ρ and ρ_s are the water density and sediment density respectively, C the volumetric sediment concentration, u_j and $u_{s,j}$ the flow velocity and sediment velocity in the x_j direction, where x_j are the Cartesian coordinates. p is the pressure, δ_{i2} the Kronecker delta, and f_i the interaction force between the fluid en sediment phase in the x_i direction. The τ and ϕ terms appear in the equations as a results of Reynolds averaging. τ_{ij} is the turbulent stress tensor in the fluid phase and $\tau_{s,ij}$ is the turbulent stress tensor for the sediment phase. ϕ_j^m, $\phi_{s,j}^{s,m}$, ϕ_i^a, and $\phi_{s,i}^{s,a}$ are turbulent fluxes. $T_{s,ij}$ is the intergranular stress tensor.

None of the three models mentions the turbulent quantities with time

derivatives, ϕ_i^a and $\phi_{s,i}^{s,a}$. Furthermore some differences are found between the models. They are summarised below.

- Dong and Zhang and Liu and Sato neglect advective terms. They refer to Dohmen-Janssen [10] to support this statement. Asano includes these terms, but substitutes the vertical momentum balances by simpler equations in order to be able to solve the set of equations.

- Asano includes drag and buoyancy in the interaction force between the fluid and the solid phase:

$$f_i = \rho C g \delta_{i2} + \frac{\rho}{2} C_D \left(\frac{\pi}{4} D^2\right) \frac{C}{\pi D^3/6} u_{i,r} \sqrt{u_r^w + w_r^2}$$

  where f_i is the interaction force in the i direction, ρ is the water density, C the sediment concentration, g the acceleration due to gravity, δ_{i2} the Kronecker delta, C_D is the drag coefficient, D is the sediment diameter, u_r is the relative horizontal velocity $u - u_s$, w_r is the relative vertical velocity $w - w_s$ and u_i is the flow velocity in the i direction. Dong and Zhang and Liu and Sato on the other hand include drag, lift, and added mass:

$$f_x = \frac{1}{2} \rho C C_D \sqrt{u_r^2 + w_r^2} u_r \frac{A_p}{V_p} + \rho C_M C \frac{D u_r}{D t}$$

$$f_z = \left(\frac{1}{2} \rho C C_D \sqrt{u_r^2 + w_r^2} w_r + \frac{\rho}{2} D C C_L |u_r| \frac{\partial u_r}{\partial z}\right) \frac{A_p}{V_p} + \rho C_M C \frac{D w_r}{D t}$$

  where A_p and V_p are the projected area and the volume of a sediment particle, C_M is the added mass coefficient and C_L is the lift coefficient.

- Asano and Dong and Zhang relate the horizontal pressure difference only

to the free stream velocity:

$$\frac{\partial p}{\partial x} = -\rho \frac{dU_w}{dt}$$

where U_w is the free stream velocity, while Liu and Sato also include a pressure gradient generating a steady current and a concentration related damping factor:

$$\frac{\partial p}{\partial x} = \frac{\partial p}{\partial x}|_{z=\delta} \left(1 - \left(\frac{C}{C_0}\right)^6\right)$$

They do so because they state that a large sediment density will hinder the transmission of pressure. Asano assumes a constant pressure gradient throughout the boundary layer.

- Asano neglects the vertical turbulent intergranular stresses $\tau_{s,zz}$ while Dong and Zhang and Liu and Sato take them into account via a direct relation to the shear stress:

$$\tau_{s,zz} = \tau_{s,xz} cot\phi$$

- The choice of parametrisation of for example the eddy viscosity and the diffusion parameter differs from one model to another.

Chapter 4

Discrete Particle Model

The DPM is a two phase Euler-Lagrange model which includes a two-way coupling between a fluid and a solid phase. The fluid phase is assumed to be a continuum, the dynamics of which can be described by the Navier-Stokes equations. The solid phase consists of discrete particles. The motion of these particles is governed by Newton's law. For the solid phase either a hard sphere or a soft sphere approach can be followed. In this study the soft sphere model is chosen because of the possible occurrence of quasi-static regions. The DPM requires a suitable collision model and a closure law for the effective momentum exchange.

4.1 Fluid dynamics

The dynamics of the fluid phase are described by the volume averaged Navier-Stokes equations. Conservation of mass is described by [19]

$$\frac{\partial(\epsilon\rho)}{\partial t} + \nabla \cdot (\epsilon\rho\mathbf{u}) = 0 \tag{4.1}$$

and conservation of momentum is given by [19]

$$\frac{\partial(\epsilon\rho\mathbf{u})}{\partial t} + \nabla\cdot(\epsilon\rho\mathbf{u}\mathbf{u}) = -\epsilon\nabla p - \mathbf{S}_P - \nabla\cdot(\epsilon\vec{\boldsymbol{\tau}}) + \epsilon\rho\mathbf{g} \tag{4.2}$$

Here $\mathbf{u}$ is the fluid velocity, ρ is the fluid density, ϵ is the local porosity, p is the fluid pressure, $\vec{\boldsymbol{\tau}}$ the viscous stress tensor, $\mathbf{g}$ the acceleration due to gravity, and $\mathbf{S}_P$ a source term representing the momentum exchange with the solid phase. This drag is described as follows [19]:

$$\mathbf{S}_P = \frac{1}{V}\int\sum_{a=1}^{N_{part}}\frac{\beta V_a}{1-\epsilon}(\mathbf{u}-\mathbf{v}_a)\delta(\mathbf{r}-\mathbf{r}_a)dV \tag{4.3}$$

$V_a/(1-\epsilon)$ gives the fraction of the volume of particle a with respect to the total local solid fraction, $\mathbf{u}-\mathbf{v}_a$ gives the relative velocity between the fluid and particle a, and the δ-function ensures that the drag force acts as a point force at the position of the particle. β is the momentum transfer coefficient, for which the drag relation of Koch and Hill [24] is used:

$$\beta_{Koch\&Hill} = \frac{18\mu\epsilon^2(1-\epsilon)}{D^2}\left(F_0(\epsilon) + \frac{1}{2}F_3(\epsilon)\,Re_p\right)$$

where μ is the fluid viscosity, ϵ the local porosity, D the particle diameter and the Reynolds particle number Re_p is given by the relation

$$Re_p = \frac{\epsilon\rho\,|\mathbf{u}_f - \mathbf{v}_p|\,D}{\mu}$$

where ρ is the fluid density and F_0 and F_3 respectively by

$$F_0(\epsilon) = \begin{cases} \frac{1+3\sqrt{\frac{1-\epsilon}{2}}+\frac{135}{64}(1-\epsilon)\ln(1-\epsilon)+16.14(1-\epsilon)}{1+0.681(1-\epsilon)-8.48(1-\epsilon^2)+8.16(1-\epsilon)^3} & if \quad (1-\epsilon) < 0.4 \\ \frac{10(1-\epsilon)}{\epsilon^3} & if \quad (1-\epsilon) \geq 0.4 \end{cases}$$

$$F_3(\epsilon) = 0.0673 + 0.212(1-\epsilon) + \frac{0.0232}{\epsilon^5}$$

This relation is valid for particle fractions ranging from 0.1 to 0.64. The Koch and Hill drag relation is an extension of the Ergun equation [16], which is one of the most widely used drag correlations in chemical engineering. This equation was empirically derived based on 640 experiments of flow through packed beds of various materials, including sand. Later the expression was improved based on Lattice-Boltzmann simulations, such as the one by Koch and Hill.

For the viscous stress tensor the general form for a Newtonian fluid is used [19]:

$$\vec{\boldsymbol{\tau}} = -(\lambda - \frac{2}{3}\mu)(\nabla \cdot \mathbf{u})\mathbf{I} + \mu(\nabla\mathbf{u} + (\nabla\mathbf{u})^T). \tag{4.4}$$

In this equation λ is the fluid phase dilatational viscosity, and $\mathbf{I}$ is the unit tensor. Note that the value of λ is, in this equation, irrelevant for liquids as they are often assumed to be incompressible. From incompressibility it follows that $\nabla \cdot \mathbf{u} = 0$ and thus the first term drops out (Bird *et al.* [4]). Furthermore, it must be noted that turbulence is not taken into account in this equation. Very close to the bed this is believed to be justified because of the high solids volume fraction which suppresses turbulence [19]. Further away from the bed turbulence is more important and can be included by means of a sub-grid scale turbulence model such as the ones by Vreman or Smagorinsky as decribed by Darmana [7]. Such a model is not included in this version of the DPM yet.

4.2 Particle dynamics

The particle motion consists of a linear and a rotational component. These are mathematically respectively described by [19]:

$$(m_a + m_{add}) \frac{d^2\mathbf{r}_a}{dt^2} = \mathbf{F}_{contact,a} + \mathbf{F}_{pp,a} + \mathbf{F}_{ext,a} + \mathbf{F}_{lubr} \tag{4.5}$$

$$I_a \frac{d\boldsymbol{\omega}_a}{dt} = \mathbf{T}_a \tag{4.6}$$

Here, m_a is the mass of particle a, m_{add} is the added mass of particle a (see below for explanation), $\mathbf{r}_a$ the position vector of particle a, I_a the moment of inertia, and $\boldsymbol{\omega}_a$ the angular velocity. The force terms represent the following. $\mathbf{F}_{contact,a}$ is the total contact force of all the individual (normal, $\mathbf{F}_{ab,n}$, and tangential, $\mathbf{F}_{ab,t}$) contact forces exerted by other particles on particle a [19]:

$$\mathbf{F}_{contact,a} = \sum_{b \in contactlist} (\mathbf{F}_{ab,n} + \mathbf{F}_{ab,t}).$$

$\mathbf{F}_{pp,a}$ is the total of inter-particle forces not included in the contact force, such as cohesive forces. Such forces were not included in this study. $\mathbf{F}_{ext,a}$ is the total of external forces on particle a, including gravity ($\mathbf{F}_{g,a}$), drag ($\mathbf{F}_{d,a}$), lift ($\mathbf{F}_{l,a}$), and fluid pressure gradients ($\mathbf{F}_{p,a}$) [19]:

$$\mathbf{F}_{ext,a} = \mathbf{F}_{g,a} + \mathbf{F}_{d,a} + \mathbf{F}_{l,a} + \mathbf{F}_{p,a}.$$

Lift forces are however not yet included in this model.

The added mass follows from the fact that if a body accelerates in a fluid the kinetic energy of the fluid changes. It depends on the shape of the body

and the density of the fluid. Because of the low density of gas it is of no importance in gas flows. In water the effect is in any case larger and possibly significant. $\mathbf{F}_{lubr}$ represents the lubrication force which accounts for proximity effects between particles and which is possibly important in liquid systems. Both added mass and lubrication forces are not yet included in this version of the DPM. A more elaborate discussion of these forces and their influence is included in chapter 6. The equation of motion used in this study is thus reduced to

$$m_a \frac{d^2\mathbf{r}_a}{dt^2} = \mathbf{F}_{contact,a} + \mathbf{F}_{ext,a} \tag{4.7}$$

Finally, $\mathbf{T}_a$ is the torque, depending on the tangential components of the contact forces [19]:

$$\mathbf{T}_a = \sum_{b \in contactlist} (R_a \mathbf{n}_{ab} \times \mathbf{F}_{ab,t}).$$

where R_a is the radius of particle a and $\mathbf{n}_{ab}$ is the normal unit vector between particles a and b.

A correct representation of contact forces ($\mathbf{F}_{contact,a}$) is rather complicated, and often a simplified model is used. In this work, a 'linear spring and dashpot model' is applied [20], the basic idea of which is shown in Figure 4.1. The centers of mass of the two particles are connected through two sets of springs and dashpots: one for the normal component of the contact force, and one for the tangential component. Furthermore, a friction slide is included to incorporate the effect of sliding in the tangential component of the contact force. In Figure 4.2 the relevant quantities for the linear spring and dashpot model are shown in the coordinate system.

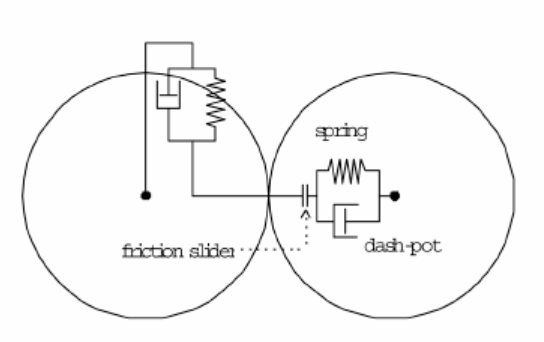

Figure 4.1: Schematic representation of the linear spring and dashpot model. This simplified model is applied for the calculation of the contact force resulting from a collision of particles. Source: Hoomans [20]

It follows that the normal contact force is calculated by ([19])

$$\mathbf{F}_{ab,n} = -k_n \delta_n \mathbf{n}_{ab} - \eta_n \mathbf{v}_{ab,n} \tag{4.8}$$

The first term on the right hand side is associated with the spring (force =

spring stiffness times distance). In this term k_n is the normal spring stiffness, δ_n the overlap between the two particles given by $\delta_n = (R_b + R_a) - |\mathbf{r}_b - \mathbf{r}_a|$, $\mathbf{n}_{ab}$ the normal unit vector as shown in Figure 4.2. The second term on the right hand side is associated with the dashpot. In this term η_n is the normal damping coefficient, and $\mathbf{v}_{ab,n}$ is the normal relative velocity. The latter quantity is defined as $\mathbf{v}_{ab,n} = (\mathbf{v}_{ab} \cdot \mathbf{n}_{ab})\mathbf{n}_{ab}$, in which

$$\mathbf{v}_{ab} = (\mathbf{v}_a - \mathbf{v}_b) + (R_a\boldsymbol{\omega}_a + R_b\boldsymbol{\omega}_b) \times \mathbf{n}_{ab}$$

The tangential component of the contact force is given by the following equations ([19]):

$$\mathbf{F}_{ab,t} = \begin{cases} -k_t\boldsymbol{\delta}_t - \eta_t\mathbf{v}_{ab,t} & for \quad |\mathbf{F}_{ab,t}| \leq \mu_f|\mathbf{F}_{ab,n}| \\ -\mu_f|\mathbf{F}_{ab,n}|\mathbf{t}_{ab} & for \quad |\mathbf{F}_{ab,t}| > \mu_f|\mathbf{F}_{ab,n}| \quad (sliding) \end{cases} \tag{4.9}$$

The upper equation should be used if no sliding occurs between the particles. In that case, the particles bounce back according to the spring and dashpot equations. If the particles slide however, the friction slider in Figure 4.1 comes into play, and the tangential contact force then depends on the magnitude of the normal contact force and a friction coefficient μ_f. The tangential unit vector $\mathbf{t}_{ab}$ shown in Figure 4.2. The equations of motion (Eq. 4.7 and Eq. 4.6) are integrated to get the position vector $\mathbf{r}_a$ and velocity vector $\mathbf{v}_a$ of particle a.

Five simulation parameters are important in this model: the linear and tangential spring stiffness k_n and k_t, the normal and tangential damping coefficient η_n and η_t, and the friction coefficient μ_f. In theory, the values of these parameters are all determined by material properties. However, in practice the

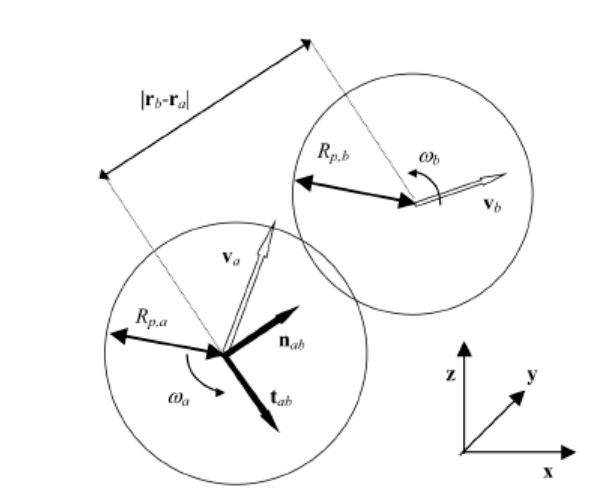

Figure 4.2: Definition of the velocity and position vectors and other relevant quantities in the coordinate system. Source: Hoomans [20]

values for the spring stiffness have to be chosen much smaller, as these values determine the contact time. A high spring stiffness results in a short contact time, which poses a significant restraint on the time step for the numerical solution [20]. As shown in Van der Hoef *et al.* [19], the damping coefficients depend on the coefficients of normal and tangential restitution e and e_t. So,

three input parameters have to specified for the collision model, and suitable values for the spring stiffness must be chosen. The values used are specified in Table 4.1. They are set to the common values (based on extensive experiments and simulations [35]) used for glass particles in discrete particle simulations.

Table 4.1: Parameter values used in the DPM

e	0.97
e_t	0.33
k_n	5000
k_t	1430
μ_f	0.1

4.3 Interphase coupling

The type of interphase coupling depends on the solid volume fraction. For high solid volume fractions ($1-\epsilon > 10^{-3}$) four-way coupling is required [19]: the interaction between the solid phase and the fluid phase, and between particles and particle-wall interactions are all important.

In the DPM particle-particle coupling is automatically accounted for in the solid phase dynamics. The interphase coupling between the fluid and the solid phase must satisfy Newton's third law. Two forces are involved in the interaction between the fluid and particles, namely the drag force exerted by the fluid on a particle, and a force associated with the pressure gradient in the fluid phase. The drag force can be expressed as [19]

$$\mathbf{F}_{d,a} = \frac{V_a \beta}{1-\epsilon}(\mathbf{u} - \mathbf{v}_a) \tag{4.10}$$

while the force due to the pressure gradient is given by [19]

$$\mathbf{F}_{p,a} = -V_a \nabla p. \tag{4.11}$$

For β the drag relation of Koch & Hill (Eq. 4.1) is used. V_a is the volume of particle a. In the fluid dynamics these forces appear in the momentum balance through $\mathbf{S}_p$ and ∇p respectively. In the momentum balance of the particle phase the forces are both included in the external force $\mathbf{F}_{ext,a}$.

4.4 Numerical implementation

The set of equations is solved numerically. For the fluid phase the scheme used is based on Patankar's SIMPLE algorithm ([30], [19]). The equations are solved on a regular (but not necessarily uniform) staggered grid. Scalar variables (e.g. pressure) are defined in the cell center, and velocity components are calculated on the sides of the cells. The grid cells should be large enough in order to let the residence time of the particles in a grid cell be several time steps at least. Furthermore, the grid should be sufficiently refined so that the sand bed contains several layers of grid cells in the vertical direction. Otherwise no velocity profile can be found in the bed.

The time step in the fluid phase system is an order of magnitude larger than the time step in the solid phase system. Due to the incompressible nature of the fluid and the small size of the particles, a very small time step of $\Delta t = 10^{-5} s$ for the fluid phase is needed for a stable simulation. For the boundary conditions a flag matrix concept is applied. This method enables one to impose arbitrary boundary conditions on every cell around the system boundaries. Internal cells

are indicated by a 1, periodic boundaries by a 9, a no slip boundary by the number 3, a free slip by the number 2, and a prescribed pressure boundary by a 5. A corner cell is labelled by the number 7 (figure 4.3).

7	5	5	5	5	5	5	7
9	1	1	1	1	1	1	9
9	1	1	1	1	1	1	9
9	1	1	1	1	1	1	9
9	1	1	1	1	1	1	9
7	3	3	3	3	3	3	7

7	5	7
2	1	2
2	1	2
2	1	2
2	1	2
7	3	7

Figure 4.3: Flag matrix concept for the boundary conditions. Left a cross section of the x-z plane, right a cross section of the y-z plane. Naturally, the number of flow cells in the actual calculation domain is much larger.

The driving force for the flow is implemented through a horizontal body force. So, instead of directly imposing a certain pressure difference over the domain, which is not possible because of the periodic boundary conditions, the pressure difference between two y-z-planes is imposed as a body force over the body between these planes. This is to the author's knowledge the only way to simulate a flow, driven by a pressure difference, with periodic boundary conditions.

4.4.1 Standard simulation settings

Unless stated otherwise, the simulation settings are as sketched in figure 4.4. The dimensions of the simulated system are 5 cm in the main flow direction (x-direction), 2.5 cm in height (z-direction), and 4 mm deep (y-direction) which is equivalent to 2 times the particle diameter. At the front and back side of

the domain a free slip boundary condition is imposed. This means that the flow does not experience stresses from the surrounding fluid. At the lower boundary a no slip boundary condition is chosen, which means that at this boundary the fluid velocity is fully slowed down by the boundary and thus zero. At the upper boundary the pressure is prescribed. The left and right hand side boundaries are periodic boundaries, which means that water and particles flowing out of the domain on the right hand side automatically flow in on the left hand side, and the other way around. They are thus directly connected. As for the particles no fixed amount was used for the simulations, but the most common numbers used are 0, 100, 500, 5000, and 25000. It must be noted that the motion of the particles is periodic in the y-direction as well. For the fluid phase this is not necessary because the thickness of the domain is only one flow cell.

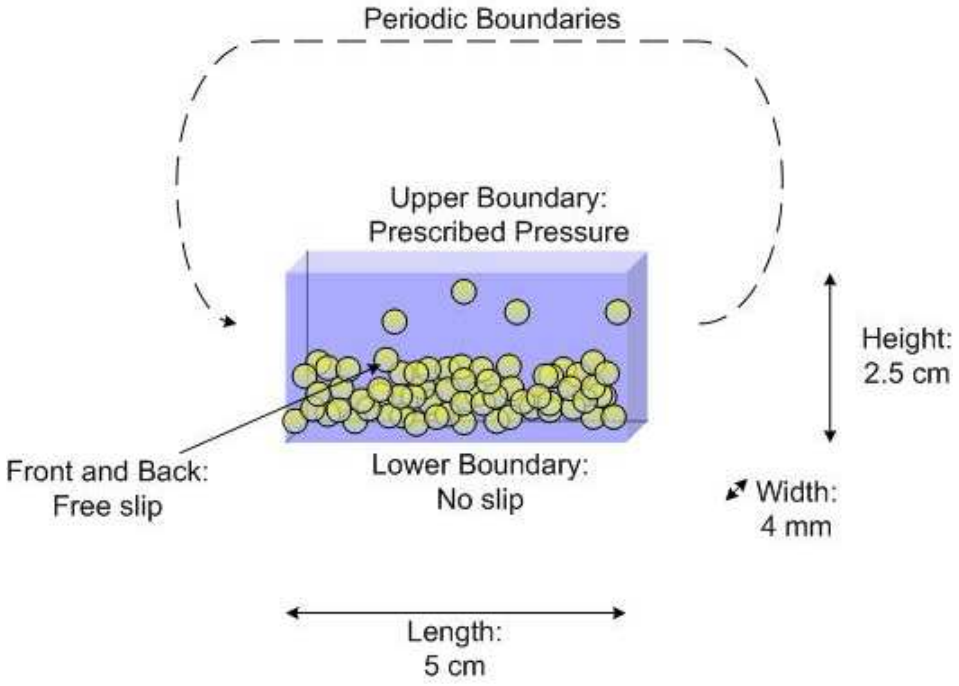

Figure 4.4: Standard simulation settings. (Particles are not to scale.)

4.5 Changes with respect to the original DPM

4.5.1 Changes in the fluid part

The DPM used in the study is usually employed for chemical engineering purposes such as the simulation of fluidised beds. The model is thus built for the simulation of a vertical gas flow in a (chemical) reactor with particles of about 0.5 mm in diameter. The main alterations to be implemented were therefore the following ones:

1. The medium of the fluid phase is changed from gas to water. This is done by choosing a fixed fluid density of $\rho = 998kg/m^3$ (as a result, a hydrostatic pressure distribution appears) and the molecular viscosity is changed to $\mu = 1.0 * 10^{-3} Pa.s$. Furthermore $\left(\frac{\partial \rho}{\partial p}\right)_T = 0$.

2. The boundary conditions are changed so that the main flow is horizontal in stead of vertical. To make this possible, periodic boundary conditions had to be added to the DPM model.

Apart from these changes, an improvement has been made as well. This is discussed in the next paragraph.

4.5.2 Improvement in the fluid part

In the original code a velocity update between the explicit part of the calculation and the calculation of the mass balance deficits was missing. Therefore the mass balance deficits were calculated using the old velocity values. Although this is not correct, the problem was never traced before because the presence of particles in the domain always makes sure the mass balance is not

satisfied before the pressure correction is made. Furthermore, the mass balance of compressible media contains the density of the fluid, while the mass balance of an incompressible fluid only depends on the velocities. If no initial disturbance is present (i.e. no particles) the calculation never reaches the implicit part of the calculation where the velocities are updated because the mass balance is already satisfied. The update is therefore necessary for a correct calculation.

The fluid part of the model is verified through a simple shear flow case (an unsteady flow profile between two parallel plates of which the upper one is set into motion) for which an analytical solution is available. This case and the results are discussed in more detail in Appendix C. After the update was added the model results provided realistic results, which are shown in figure 4.5. In this figure the simulation results are plotted together with analytical results for several time intervals.

4.5.3 Changes in the particle part

The only change made to the particle part of the DPM is the possibility of periodicity of the particles. For gas fluidisations in reactors this is not necessary as the particles will all stay in the domain at all times. In the case of sediment transport the particles will pile up on the right side of the domain, while they should flow out of it. Any particle moving out of the domain in either horizontal direction now directly flows in on the other side of the domain. The number of particles is thus preserved, while they can still move freely in and out of the calculation domain.

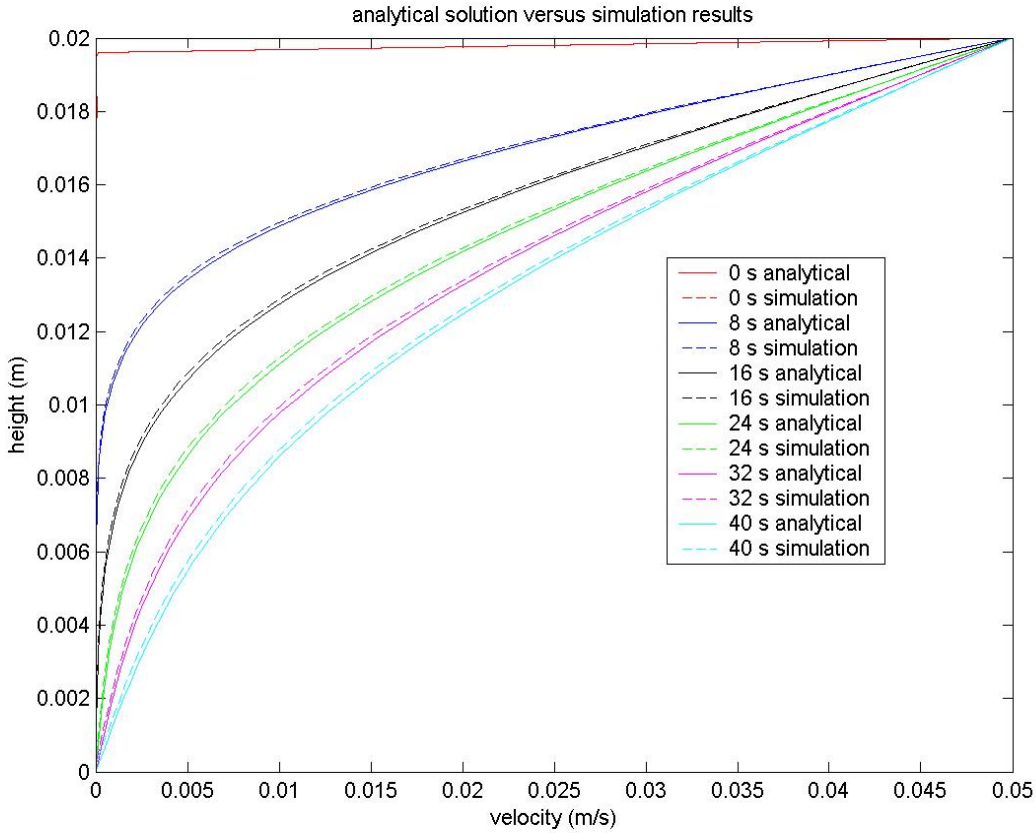

Figure 4.5: Comparison of the analytical solution (solid lines) and the simulation results (striped lines) for laminar shear flow. No particles involved.

4.6 Requirements on initial and boundary conditions

4.6.1 Influence of upper boundary condition

For the upper boundary condition three kind of boundary conditions can be chosen: no-slip, free slip, and prescribed pressure. The no-slip boundary condition is not very realistic, as it implies that the water experiences the same shear from water as from the sediment bed. By contrast, free slip and prescribed pressure both allow for increasing velocity with height above the bed. In the simulation a prescribed pressure boundary condition is used. In this section it is explained why the prescribed pressure is chosen over free slip.

Simulations were run for both boundary conditions until the flow was steady. The particles were left out for an unbiased result. The resulting time averaged velocity profiles are plotted in figure 4.6. In the left panel of this figure the upper boundary condition is free slip, in the right panel the upper boundary condition is prescribed pressure. All other characteristics are the same. In the case of prescribed pressure, the flow in the upper part of the computational domain is slowed down a little. This is probably a result of Bernoulli's law: the velocity increases because of the horizontal acceleration imposed on the flow. This causes the pressure to decrease, but the pressure on the upper boundary is fixed. The only solution is thus a lower flow velocity.

Based on the velocity profile one would be inclined to choose for the free slip boundary condition. However, for reasons unknown the model's iterative part does not converge for cases with free slip on the upper boundary condition if more than about 100 particles are involved. Therefore, despite

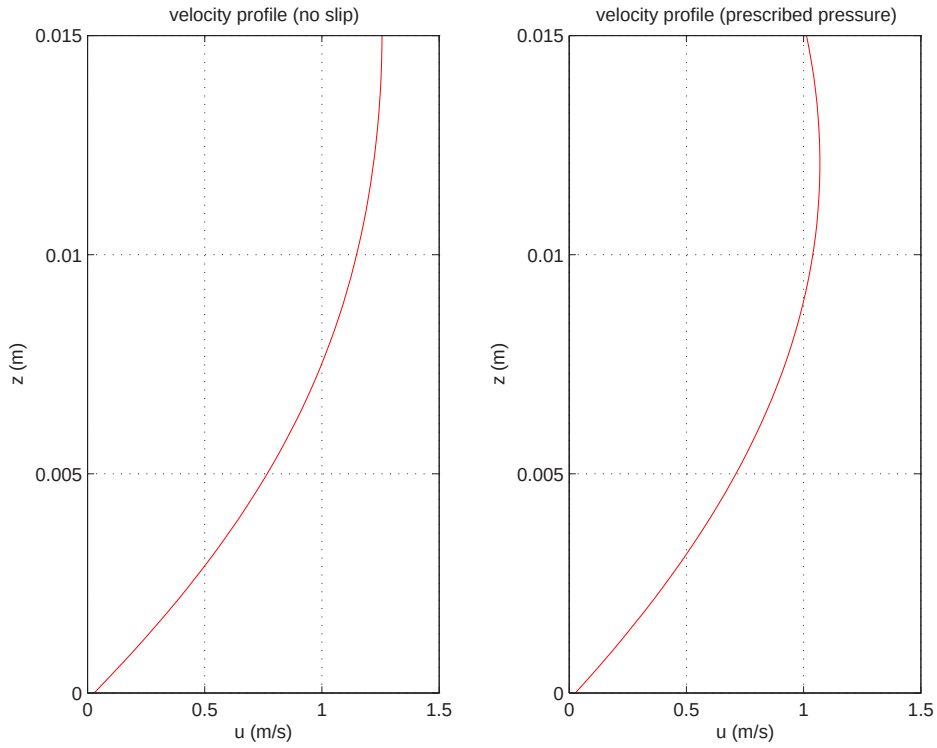

Figure 4.6: Velocity profiles for steady flow with different upper boundary conditions (no particles). Left panel: free slip. right panel: prescribed pressure. (No particles involved.)

the somewhat strange decreasing velocity in the upper region of the computational domain, all simulations were performed with a prescribed pressure on the upper boundary.

4.6.2 Influence of initial velocity profile

For the simulation of a steady flow it is desirable to let the velocity profile converge to a steady flow as soon as possible, in order to minimise the runtime of the simulation. The choice of initial velocity profile is crucial in this respect. As is shown in figure 4.7 a steady flow is reached much faster with a linear velocity profile than in the case of a uniform velocity profile. The convergence

rate is here defined as

$$\frac{\sum_i \left| |u_i^n| - \left|u_i^{n-1}\right| \right|}{NX * NZ}$$

where the sum is over i flow cells and calculated for n time intervals. $NX$and NZ are the number of flow cells in the x and z direction respectively.

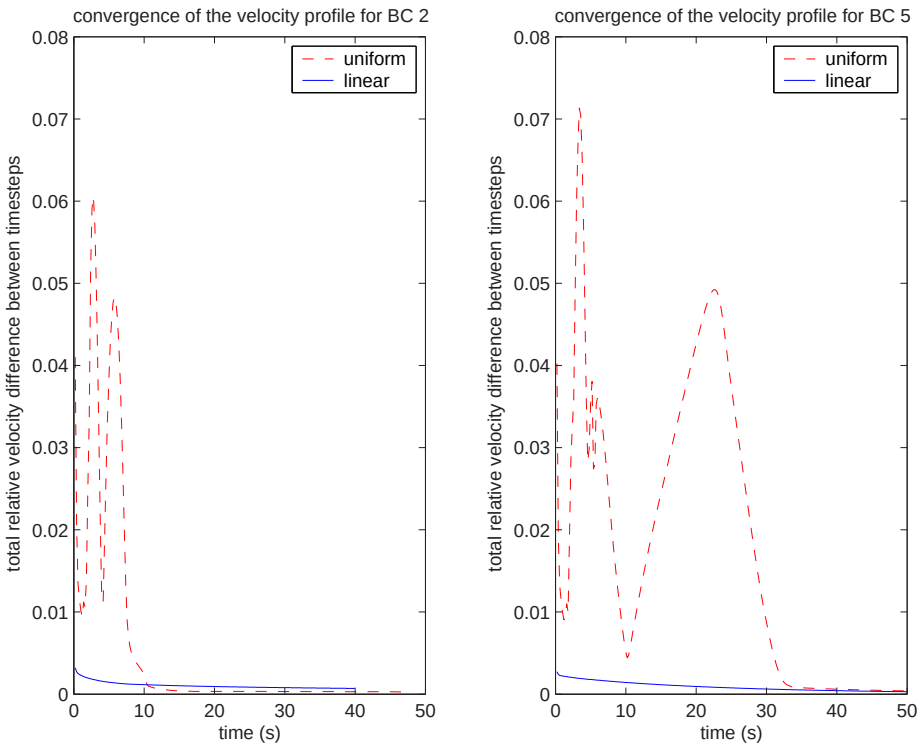

Figure 4.7: Rate of convergence to a steady velocity profile with different upper boundary conditions. Left panel: free slip. right panel: prescribed pressure. The blue line gives the convergence rate in case the initial velocity profile is linear, the red line for a uniform one. (Number of particles = 100.)

Chapter 5

Results

5.1 Results for fluid phase only

Although we did not succeed in simulating sheet flow with the DPM, some results are worth discussing. As a first step steady flow without particles was simulated with the DPM for several reasons:

- to study the behaviour of the DPM for incompressible flow
- to study the relation between the imposed horizontal body force and the steady depth averaged flow velocity
- to study the convergence of the velocity profile from the initially imposed profile to the final velocity profile

As stated in chapter 4 incompressible flow simulations with the DPM are only possible under certain conditions. The flow solver alone seems to work properly. As shown in figure 4.5 the results are good, though no perfect agreement with the analytical solution is found (grid refinement might resolve this).

However, as soon as particles are introduced into the system the possibilities of the DPM are limited. For example, simulations only run with a prescribed pressure boundary condition on the upper side, while free slip would be preferable. Also, the magnitude of the horizontal body force imposed on the flow as a driving force is limited to values of an order of magnitude smaller than 1 to ensure stability.

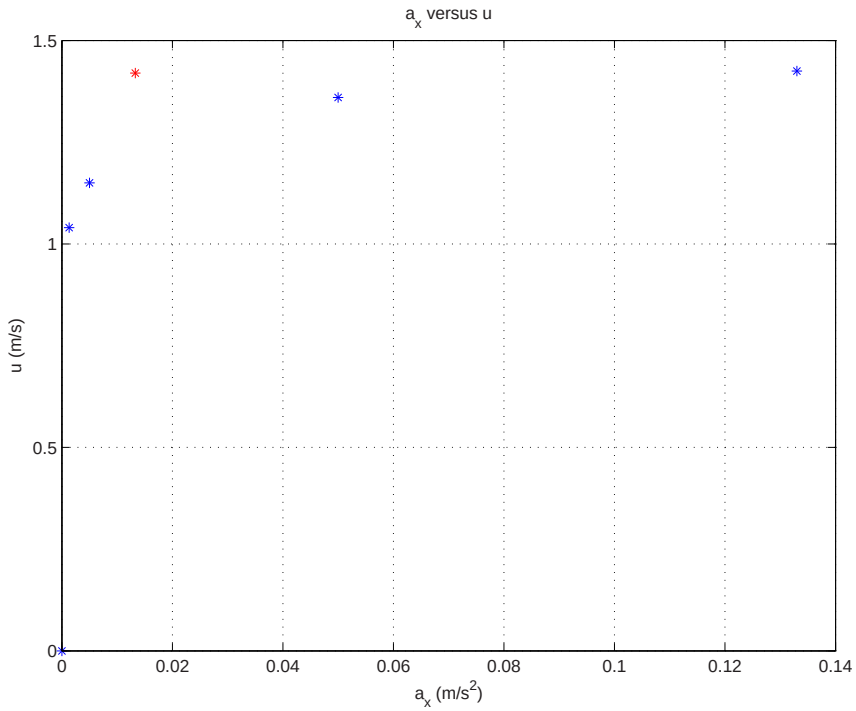

Figure 5.1: Relation between horizontal acceleration and horizontal flow velocity.

In figure 5.1 the relation between the value of the horizontal acceleration a_x and the resulting horizontal velocity in a steady flow is given. The value for $a_x = 1.3 * 10^{-2} m/s^2$ (marked red) is remarkable, as the resulting velocity is higher than the velocities for higher accelerations. Furthermore, for higher values of the acceleration the velocity hardly increases. To study this in more detail, figure 5.2 gives the development of the depth averaged velocities in

time for different values of a_x. The development of the velocity for $a_x \geq 5.0 * 10^{-2} m/s^2$ is very different from the other lines in the graph. In these lines first an overshoot of the velocity is observed after which the velocity is rectified to its final value while for smaller accelerations the profiles converge smoothly to their steady state value. Through this mechanism the convergence is much faster than in the low-value acceleration range. On the other hand, as figure 5.3 shows, the convergence of these simulations is much more capricious and does not turn to zero but to a higher (though steady) value. This indicates probably a different flow regime, though the large deviations could also have a numerical origin.

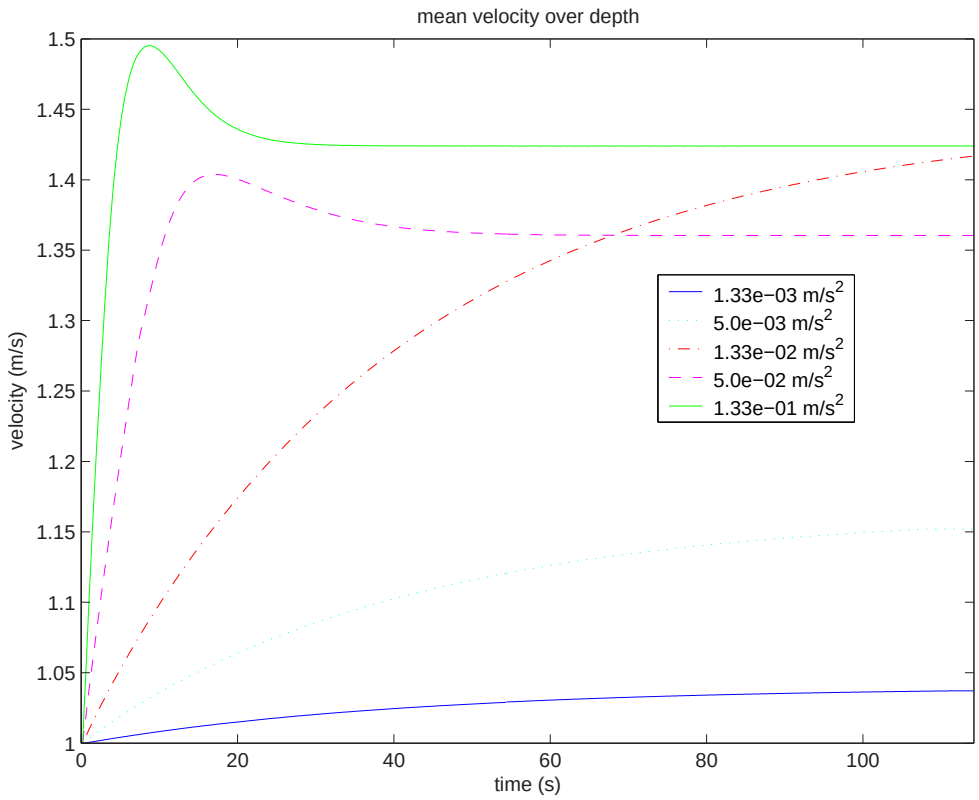

Figure 5.2: Development of the velocity in time for different values of the horizontal acceleration.

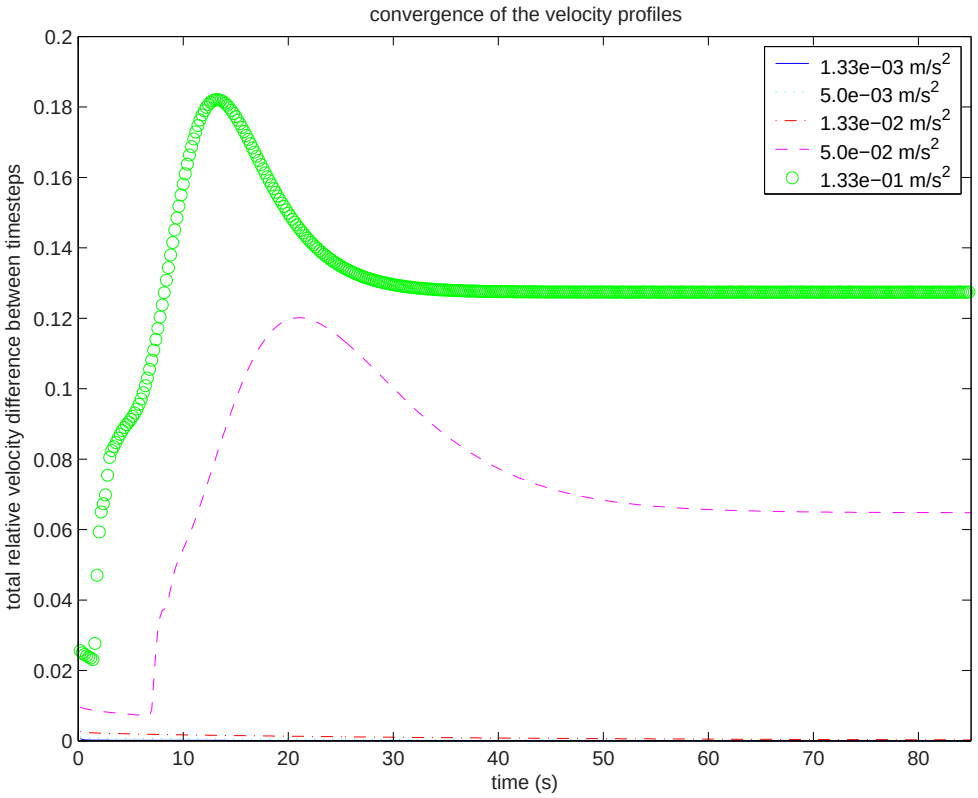

Figure 5.3: Convergence of the velocity profiles for different values of the horizontal acceleration.

Apart from the form of the convergence graphs, the time it takes for the velocity to reach its steady state value is very interesting. Unfortunately, for all values of a_x in the simulated range the convergence time is extraordinary long, i.e. in the order of 60 seconds (for small horizontal body forces even more). Given the fact that the time it takes to simulate such a time period, even without particles involved, is about two weeks, this is actually unacceptable. Moreover, from this we must conclude that wave simulations in the range of any practical importance (wave periods of 4 to 12 seconds) cannot be made using this model in this stage. A test simulation confirmed that na realistic flow velocities are obtained.

Other results of interest are the pressure distribution (figure 5.4) and the velocity profile (figure 5.5). As a result of the constant density a hydrostatic pressure profile is found. The velocity increases from zero at the no-slip bottom boundary to maximum on the upper boundary. Note that only a small part of the domain in the horizontal direction is plotted in the velocity vector plot.

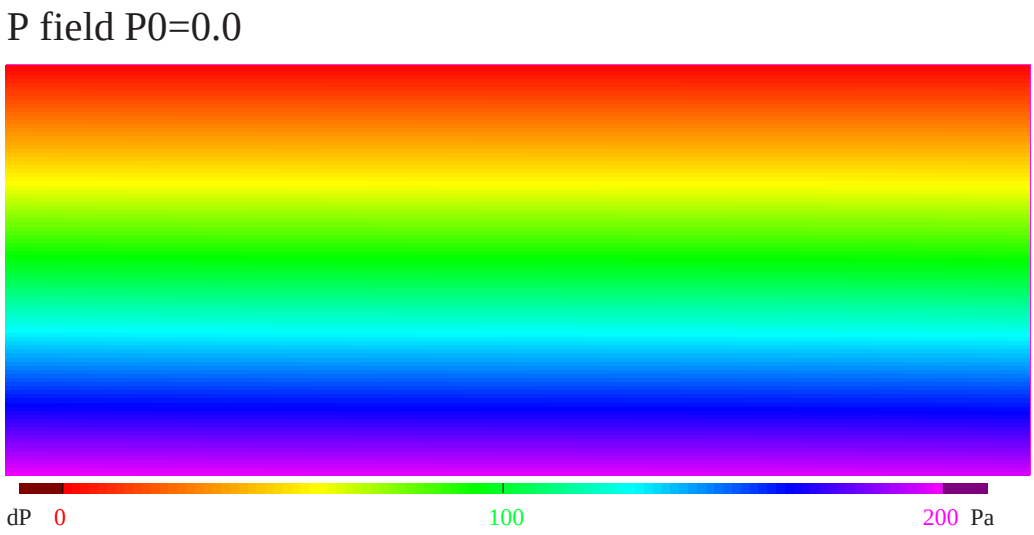

Figure 5.4: Hydrostatic pressure.

5.2 Full DPM results

Simulations were run with 5000 particles to see the general behaviour of the particles in a steady flow, according to the DPM. The particles were put into the calculation domain in a neatly ordered fashion (figure 5.6(a)). Directly after the start of the simulation the grains fall down and form a dense layer of particles. This process takes about 0.5 s (figure 5.6(d)), which is equivalent to about three days of simulation time.

It turned out that the particles lay steady on the floor without moving for

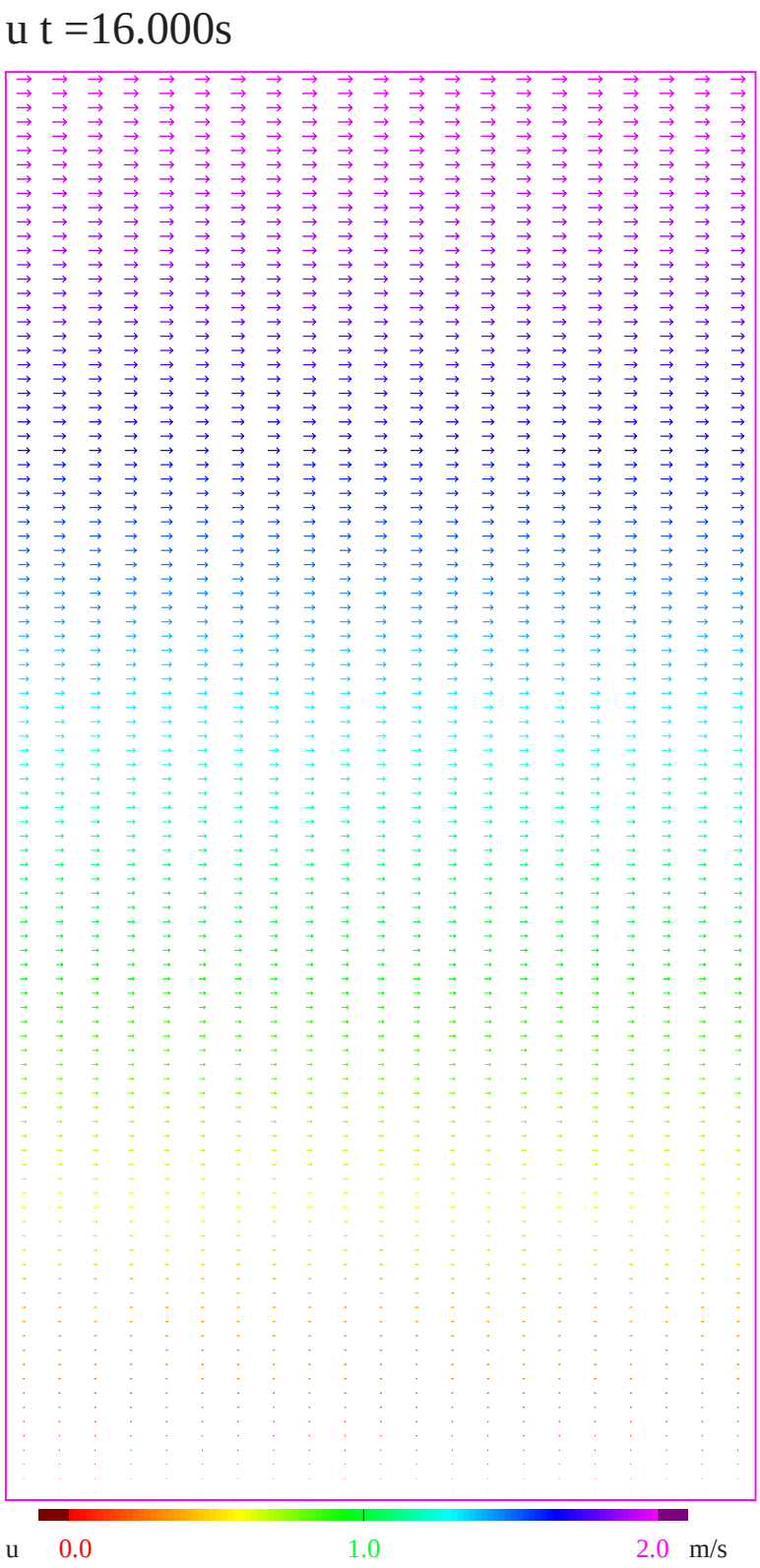

Figure 5.5: Velocity profile.

a_x is $O\left(10^{-2}\right)$ or less (figure 5.7), and the particles slid as a block over the bottom for a_x is $O\left(10^{-1}\right)$ (figure 5.8). This is probably caused by the lack of friction provided by the flat and slippery bottom. A way to impose more friction would be to fix a layer of sediment grains on the bottom.

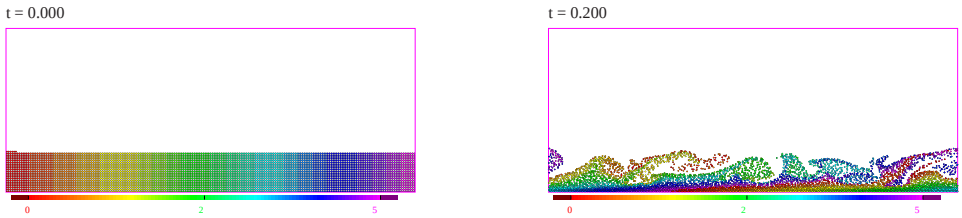

(a) t = 0.0 s (b) t = 0.2 s

(c) t = 0.4 s (d) t = 0.6 s

Figure 5.6: The initial settling of the grains. The colour indicates the original horizontal position of the particle.

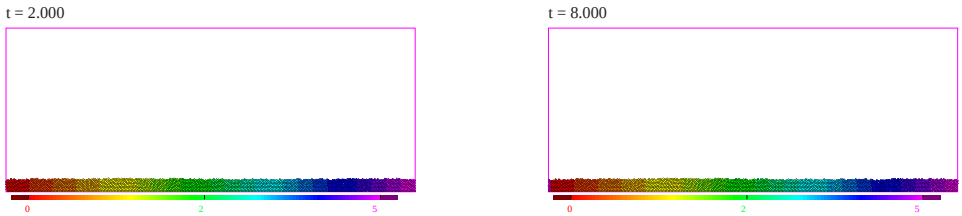

(a) particle positions after t = 2 s (b) particle positions after t = 8 s

Figure 5.7: No sediment movement

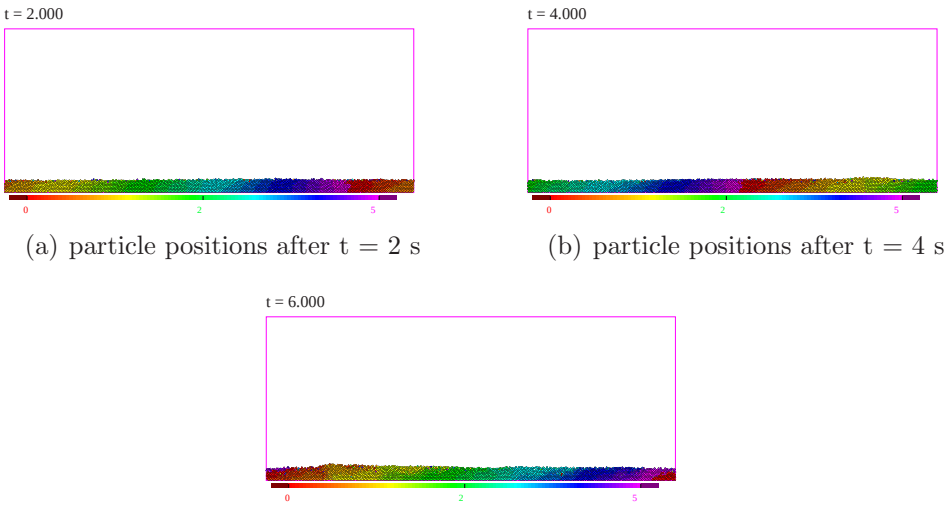

(a) particle positions after t = 2 s

(b) particle positions after t = 4 s

(c) particle positions after t = 6 s

Figure 5.8: The particles slide as one block over the floor. The colour of the particles indicates their horizontal position at t = 2s.

Chapter 6

Discussion

6.1 Inventory of uncertainties and shortcomings

Uncertainty is inherently involved in modelling practice. Although not every type of uncertainty can be excluded or even diminished, it is important to acknowledge the sources of uncertainty and try to estimate their influence on the model results. Besides, in this case an exploration of uncertainties can shed some light on the weak points of the model and its underlying assumptions and thereby give some starting-points for further research.

Before starting the actual analysis it is important to realise two issues. First, the DPM used for this study has proven to be very accurate in its original form and for its original purposes. It would therefore be meaningless to re-evaluate every aspect of the model. Rather we will focus on the differences we made in the model itself, as well as on the differences in the natural system the model is used to represent (sediment transport versus gas fluidisations).

Second, due to the complexity of the model (and the run time inherently involved), and the limited time span available for this explorative study, a complete uncertainty analysis as for example outlined by Van der Klis [36] is not feasible. Here only an inventory of the uncertainties involved an a qualitative estimate of their influence is made, leaving further analysis to future research.

Uncertainties manifest themselves in several locations. Walker [38] defines the following ones:

1. Uncertainty in the context of the model
2. Model uncertainty (model structure uncertainty and model technical uncertainty)
3. Uncertainty in model input (external driving forces and system data)
4. Uncertainty in model parameters
5. Model outcome uncertainty, which is the accumulated uncertainty of all the above

The first four of the above locations are discussed below.

1. The context of the model is associated with uncertainties is the initial and boundary conditions. Initial conditions do not influence the final results, only the rate of convergence. In the boundary conditions the upper boundary introduces some uncertainty into the model. On the upper boundary the pressure is prescribed and assumed constant. If the upper boundary would be air, this would be no doubt the best choice. However, in our case the upper boundary of the simulated system is

the water above. Assuming hydrostatic pressure, the pressure would indeed be constant. If dynamic pressure changes are important however, this will be different. Furthermore the periodic boundaries introduce uncertainties as numerical variations are preserved within the calculation domain.

2. The model uncertainty comprises several items:

   - *Spherical particles are used*

     The DPM uses perfectly spherical particles. In chemical engineering this is only a minor issue as the particles used in experiments as well as the real particles used in the industry are spherical or at least nearly spherical. Sand grains however are anything but spherical. This will influence the model (as it is) in two aspects:

     – The drag relation is different for non-spherical particles

     – Collisions between spherical particles differ from collisions between non-spherical particles

     Moreover, it puts a restraint on the applicability of a part of the model still to be made. The added mass force namely depends on the shape of the particles, as does the extent in which lubrication forces are important as will be explained later on.

     The assumption of spherical particles is clearly essentially wrong as we know for a fact that the particles are not spherical. However, models for irregularly shaped particles do not exist. Shape effects can partially be included by a shape factor in the drag relation, but for the collision model there is no alternative. Note that shape

effects are hardly accounted for in existing sheet flow models either, only a shape factor is sometimes used.

- *The added mass is not taken into account*

  This will on itself influence the results, though the magnitude of its influence is difficult to estimate. Taking into account added mass in the model however is not as straightforward as it might seem. Only if the flow would be an irrotational potential flow and if the assumption of spherical particles would be valid, an easy analytical expression exists for the added mass force [40]. However, neither of these preconditions are met for sediment sheet flow. For irregular shapes such as sand grains all 36 components of the added mass tensor must be defined which are different for every particle and moreover generally not identifiable or even proven to be zero [5]. This makes it very hard to estimate the influence of added mass on the behaviour of sand particles.

- *Lubrication forces are not taken into account*

  Lubrication forces appear as a result of the proximity of two planes pushing the fluid in between away and sucking the fluid back when the distance grows. If we take two spherical particles, let the distance which separates them decrease, and zoom in on the contact point, this can be schematised by two flat plates approaching each other (as long as we would zoom in far enough). This would be the same for every contact point if the particles are perfectly spherical. However, if a sharp-edged sand grain collides with another sharp-edged sand grain, the lubrication force would be negligibly small.

On the other hand, if two sand grains collide facing their flat sides, the lubrication force will be significantly larger than for spheres.

- *Lift forces are not included in the DPM*

  The lack of lift forces in the interaction forces makes it harder for the flow to pick up particles from the bed. This force should not be left out, as some authors claim that it is important ([13], [25]) while others do not even mention it [1]. Including lift forces in the DPM could clarify the issue.

- *The sub-grid-scale turbulence is neglected*

  Sub-grid-scale turbulence is not expected to be important very close to the bed as turbulence is heavily suppressed by the highly concentrated particles. However, the height above the bed from where it should be included is not known. Even more, that is exactly an issue that could be investigated using a DPM. It is possible to include sub-grid-scale turbulence by a SGS-turbulence model. The effect of not including sub-grid-scale turbulence is difficult to estimate. The flow cells are very small, so turbulence is accounted for up to a very small scale. Whether or not they are sufficiently small depends on the grid size with respect to the Kolmogorov length scale.

- *An algorithm for compressible flow is used for the simulation of an incompressible flow*

  In principle an arbitrary equation of state can be chosen in the model. Experience has shown however that the model, if used to simulate incompressible flow, is extremely slow and for some cases does not work at all. As in gases the density is a function of pressure,

this could cause the method to be less flexible for incompressible flows and this could be a possible explanation for the refusal of the model to convergence in several cases and also for the large convergence time in steady flow. This remains however speculation at this stage.

3. Uncertainty in model input comprises uncertainty in external driving forces and in system data. The latter is irrelevant in this study, while the former is found in the way the flow is driven, i.e. in the magnitude of the horizontal body force and the exact relation between this body force and the pressure difference as measured in experiments.

4. Several parameters are subject to uncertainty:

   - *Simulation parameters in the collision model (e, e_t, k_n, k_t, and μ_f).* The values of these parameters are extensively studied in previous studies through experiments and simulations. As they are simulation parameters and not physical parameters, their value should not influence the model results. Naturally care is still required in this respect.

   - *Momentum transfer coefficient β*

     β contains quite some uncertainty. Especially the effect of irregularly shaped particles on the drag relation is inconvenient. The drag relation used is in any case valid for the whole range of void fractions ϵ occuring in sheet flow.

   - *The water density ρ*

     For the water density ρ the probability of large variations is neg-

ligible. It should be noted that in the model simulation the fresh water value in stead of the salt water value is used. The effect of this faulty value is not expected to have any significant effect on the simulation results.

- *The viscosity of water* μ

  The water viscosity μ will not display variations within the time window of the simulations. However, the value is different in summer and winter due to temperature differences (about a factor 2). The same goes for water density, but the difference here is very small ($2kg/m^3$ on a total of about $1030kg/m^3$) [34].

6.2 Strong and weak points of the DPM

A major strong point of the DPM is the level of detail provided in the results, both with respect to space and time as well as the number of physical quantities output is provided about. This ensures the results can be well studied. Another important strong point is the full four-way coupling. This ensures that the influence of the particles on the water, the influence of the water on particles and the mutual influence of particles during collisions is all accounted for, which is crucial in high particle concentrations.

The most obvious weak point of the DPM is the constraint put on the spatial and temporal extent of the simulations. Unfortunately that is the price that must be paid for the level of detail. A weak point of this particular model is the use of compressible scheme in the flow solver, which, although in principle this should work for incompressible flows, seems to raise some difficulties. A weak point in general is the use of spherical particles, which

goes for all sediment transport models.

Chapter 7

Conclusions & recommendations

7.1 Conclusions

With the results obtained in this study the research questions can be answered. They will now be addressed one at the time.

Which points of dispute in existing sheet flow models could be studied with the help of a DPM?

The literature review on sheet flow models revealed that roughly three types of models can be distinguished. In order of increasing level of detail they are the Transport Formulae, the Reynolds Averaged Navies Stokes models and the Discrete Particle Models. Of all three types of models several examples can be found in literature. Several discrepancies exist between different models of the same type. The DPM can best be used to study the ones in the two-phase continuum RANS models, as they most closely resemble the DPM and are also based on physical principles. Examples of issues that can be studied with the help of a DPM are which interaction forces have to be included, which as-

sumptions should be made for a correct description of the fluid pressure, which turbulent stresses and fluxes are important and how they can best represented, and which parametrisation for the eddy viscosity and sediment diffusivity are most accurate.

Can this DPM simulate horizontal sediment movement in water? If so, how does it perform in simulating sheet flow?

Provided a prescribed pressure boundary condition is imposed on the upper boundary and the value of the horizontal acceleration representing the horizontal pressure difference is well chosen, the DPM is able to simulate the horizontal movement of spherical particles. However, in a steady state situation, the particles slide as one block over the bottom due to lack of friction. Another problem is the sensitivity of the flow solver. That is, the upper boundary condition must be prescribed pressure, otherwise convergence of the iterative calculation is impossible. This raises the question to what extent this particular scheme is suitable for simulations of incompressible flows.

Adding friction to the bottom (for example by fixing the lower level of particles on the bottom) will probably solve the problem of sliding sediment. The issue of the flow solver, whether the problem indeed lies in the nature of the numerical scheme or not, is not expected to be solvable within this version of the DPM. It is expected that simulating a sheet flow like behaviour will be possible with this model if more time is spent on completing the model and increasing the amount of friction on the bottom. This time may though be better spent in starting with a code that has already proven to perform well for incompressible flows. It must be noted that the simulation of oscillatory sheet flow in wind waves is impossible as the convergence time is extraordinary

long, which makes the plea for a different model even stronger.

7.2 Recommendations

Further research should focus on the following issues:

- As the potential value of a well working DPM for sheet flow sediment transport is very high, further attempts to make such a model are highly encouraged.
- It is recommended to try and start with a flow solver for incompressible flows [1] and see whether or not the simulations are more stable and whether the simulation time can be considerably reduced. Also the rate of convergence should be studied.
- The influence of added mass and lubrication forces should be investigated further, in particular in relation to the effect of irregular shapes of the particles. Also lift forces should be added as one of the interaction forces.
- It is recommended to include sub-grid-scale turbulence model for a complete representation of the flow above and in the sheet flow layer.
- In order to study the difference between the behaviour of spherical and non-spherical particles experiments with spherical glass particles should be carried out and compared to the experimental results of similar sand experiments.

[1] The model made by Ir. Dijkhuizen of the FCRE group could be used as a starting point.

Bibliography

[1] T. Asano. Two-phase flow model on oscillatory sheet-flow. In *Proceedings of 22ns International Conference on Coastal Engineering, ASCE*, pages 2372–2384, 1990.

[2] R.A. Bagnold. Experiments on a gravity-free dispersion of large solid spheres in a newtonian fluid under shear. *Proc. R. Soc. London*, A 225:49–63, 1954.

[3] R.A. Bagnold. Mechanics of marine sedimentation. In M.N. Hill, editor, *The Sea*, volume 3. Interscience, New York, 1963.

[4] R.B. Bird, W.E. Steward, and E.N. Lightfoot. *Transport Phenomena*. John Wiley and Sons, New York, 2002.

[5] C.E. Brennen. A review of added mass and fluid inertial forces. Technical Report CR 82.010; N62583-81-MR-554, Naval Civil Engineering Laboratory, Port Hueneme, California, USA, January 1982.

[6] H.H. Chang. *Fluvial Processes in River Engineering*. Krieger Publising Company, Malabar, Florida, 1992.

[7] D. Darmana. *On the multiscale modelling of hydrodynamics, mass transfer and chemical reactions in bubble columns.* PhD thesis, University of Twente, 2006.

[8] A.G. Davies and Z. Li. Modelling sediment transport beneath regular symmetrical ans asymmetrical waves above a plane bed. *Continental Shelf Research*, 17(5):555–582, 1997.

[9] M. Dibajnia and A. Watanabe. Sheet flow under nonlinear waves and currents. In *Proc. 23rd Int. Conf. on Coast. Eng.*, pages 2015–2028, Venice, 1992.

[10] C.M. Dohmen-Janssen. *Grain size influence on sediment transport in oscillatory sheet flow: phase lags and mobile bed effects.* PhD thesis, TU Delft, 1999.

[11] C.M. Dohmen-Janssen, W.N. Hassan, and J.S. Ribberink. Mobile-bed effects in oscillatory sheet flow. *Journal of Geophysical research*, 106, No C11:27,103–27,115, November 15, 2001.

[12] C.M. Dohmen-Janssen, D.F. Kroekenstoel, W.N. Hassan, and J.S. Ribberink. Phase lags in oscillatory sheet flow: experiments and bed load modelling. *Coastal Engineering*, 46:61–87, 2002.

[13] P. Dong and K. Zhang. Two-phase flow modelling of sediment motinos in oscillatory sheet flow. *Coastal Engineering*, 36:87–109, 1999.

[14] P. Dong and K. Zhang. Intense near-bed sediment motion in waves and currents. *Coastal Engineering*, 45:75–87, 2002.

[15] T.G. Drake and J. Calantoni. Discrete particle model for sheet flow sediment transport in the nearshore. *Journal of Geophysical Research*, 106(C9):19859–19868, September 15 2001.

[16] S. Ergun. Fluid flow through packed columns. *Chemical Engineering Proceedings*, 48:89, 1952.

[17] H. Gotoh and T. Sakai. Numerical simulation of sheetflow as granular material. *Journal of Waterway, Port, Coastal, and Ocean Engineering*, pages 329–336, November/December 1997.

[18] K. Guizien, C.M. Dohmen-Janssen, and G. Vittori. 1dv bottom boundary layer modeling under combined wve and current: Turbulent separation and phase lag effects. *Journal of Geophysical Research*, 108(C1):3016, 2003. doi:10.1029/2001JC001292.

[19] M.A. van der Hoef, M. Ye, M. van Sint Annaland, A.T. Andrews IV, S. Sundaresan, and J.A.M. Kuipers. Multi-scale modeling of gas-fluidized beds. *Advances in Chemical Engineering*, 31:65–149, 2006.

[20] B.P.B. Hoomans. *Granular dynamics of gas-solid two-phase flows.* PhD thesis, University of Twente, 1999.

[21] T.J. Hsu, J.T. Jenkins, and P.L.F. Liu. On two-phase sediment transport: Sheet flow of massive particles. *Proc. R. Soc. London*, A 460:2223–2250, 2004.

[22] A. Lamberti, L. Montefusco, and A. Valiani. A granular-fluid model of the stress transfer from fluid to the bed. In Soulsby and Bettess, editors,

Euromech 262, Sand transport in Rivers, Estuaries and the Sea., pages 209–220. Balkema, Rotterdam, 1990.

[23] Z. Li and A.G. Davies. Towards predicting sediment transport in combined wave-current flow. *Journal of Waterway, Port, Coastal, and Ocean Engineering*, pages 157–164, July/August 1996.

[24] J.M. Link. *Development and Validation of a Discrete Particle Model of a Spout-Fluid Bed Granulator.* PhD thesis, University of Twente, 2006.

[25] H. Liu and S. Sato. Modeling sediment movement under sheetflow conditions using a two-phase flow approach. *Coastal Engineering Journal*, 47(4):225–284, 2005.

[26] H. Liu and S. Sato. A two-phase flow model for asummetric sheetflow conditions. *Coastal Engineering*, 53:825–843, 2006.

[27] O.S. Madsen and W.D. Grant. Quantitative description of sediment transport by waves. In *Proc. 12th Int. Conf. on Coast. Eng.*, pages 1093–1112, 1976.

[28] T. O'Donoghue and S. Wright. Concentration in oscillatroy sheet flow for well sorted and graded sands. *Coastal Engineering*, 50:188–138, 2003.

[29] T. O'Donoghue and S. Wright. Flow tennel measurements of velocities and sand flux in oscillatory sheet flow for well-sorted and graded sands. *Coastal Engineering*, 51:1163–1184, 2004.

[30] S.V. Patankar and D.B. Spalding. A calculation procedure for heat, mass and momentum transfer in three-dimensional parabolic flows. *International Journal of Heat and Mass Transfer*, 15:1787–1806, 1972.

[31] J.S. Ribberink. Bed-load transport for steady flows and unsteady oscillatory flows. *Coastal Engineering*, 34:59–82, 1998.

[32] J.S. Ribberink and A.A. Al-Salem. Sediment transport in oscillatory boundary layers in cases of rippled beds and sheet flow. *Journal of Geophysical Research*, 99(C6):12707–12727, 1994.

[33] J.S. Ribberink and A.A. Al-Salem. Sheet flow and syspension of sand in oscillatory boundary layers. *Coastal Engineering*, 25:205–225, 1995.

[34] R. Soulsby. *Dynamics of marine sands.* Thomas Telford Services Lim., London, 1997.

[35] M.A. Van der Hoef. Private communication.

[36] H. Van der Klis. *Uncertainty analysis applied to numerical models of river bed morphology.* PhD thesis, Delft University of Technology, 2003.

[37] G. Vittori. Sediment suspension due to waves. *Journal of Geophysical Research*, 108(C6):3173, 2003. doi:10.1029/2002JC001378.

[38] W.E. Walker, P. Harremoës, J. Rotmans, J.P. van der Sluijs, M.B.A. van Asselt, P. Janssen, and M.P. Krayer von Krauss. Defining uncertrainty: A conceptual basis for uncertainty management in model-based decision support. *Integrated Assessment*, 4(1):5–17, 2003.

[39] K.C. Wilson. Analysis of bed-load at high shear stress. *Journal of Hydraulic Engineering*, 113(1):97–103, January 1987.

[40] C. Yih. *Fluid mechanics: a concise introduction to the theory.* McGraw-Hill Inc., New York, 1969.

Appendix A

Sheet flow models

Several existing sheet flow models were studied for their similarities and differences. In the following sections an overview is presented of several transport formulae, RANS models and discrete particle models for steady as well as for oscillatory flow. At the end of each section on a model type a summary of the findings is given.

A.1 Transport formulae

A.1.1 Steady flow models

Wilson (1987)

For steady flow Wilson proposes:

$$q_s = \frac{11.8}{g(s-1)} \left(\frac{\tau}{\rho} \right)^{1.5} \tag{A.1}$$

where q_s is the sediment transport rate per unit of width, g is the acceleration due to gravity, $s = \rho_s/\rho$ is the relative sediment concentration (ρ_s and ρ are

the density of the sediment and water respectively). The shear stress τ consists of a fluid-related and a particle-related part:

$$\tau = \tau_f + \tau_s$$

- $\tau_f = \tau(1 - \frac{\tau_s}{\tau}) = \tau(1 - \int_{\eta}^{\eta_0} C_r d\eta)$

  C_r is the ratio of the local solids concentration C and the loose-poured volumetric solids concentration in the bed C_b. $\eta = y/y_s$, where y_s is the height above the bed where $\tau_f = 0$. $\eta_0 = \delta_s/y_s$, where δ_s is the sheet flow layer thickness (at $y = \delta_s : \tau_s = 0$).

  From Dohmen-Janssen [10]: $\tau_f = \rho\nu_e \frac{\partial \bar{u}}{\partial z}$ where ν_e is the turbulent eddy viscosity.

- $\tau_s = \sigma_s \tan\phi'$

  Here σ_s is the intergranular normal stress given by

  $\sigma_s = \int_y^{\delta_s} g\rho(s-1)C_b C_r dy$

  and ϕ' is the dynamic friction angle of the solids.

A schematisation of the reference levels as used by Wilson is given in figure A.1.

Ribberink (1998)

Meyer-Peter and Mueller derived a type of transport formula that forms the basis for all sheet flow transport formulae nowadays. The theoretical basis for this type of formula in sheet flow conditions was given by Wilson in 1992.

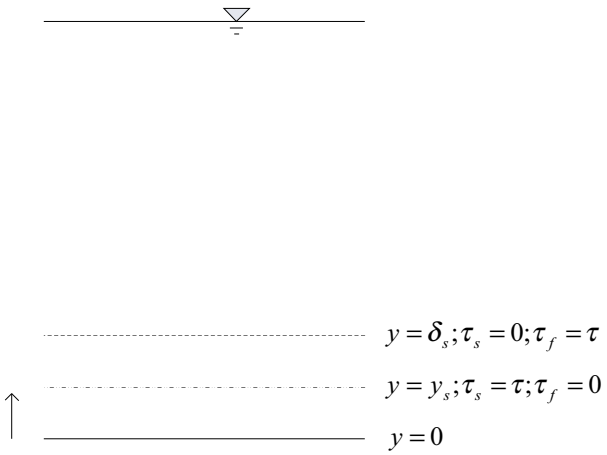

Figure A.1: Position of reference levels in the geometry used by Wilson [1987]

The formula reeds

$$\Phi_b = \begin{cases} m(\theta' - \theta_{cr})^n & \theta' \geq \theta_{cr} \\ 0 & \theta' < \theta_{cr} \end{cases} \tag{A.2}$$

Here Φ_b is the non-dimensional bed load transport given by

$$\Phi_b = \frac{q_b}{\sqrt{\Delta g D_{50}^3}}$$

where $\Delta = (\rho_s - \rho)/\rho$ is the relative sediment concentration, m is a parameter and n is a constant. θ_{cr} is the critical Shields parameter for sediment motion, and θ' is the effective Shield's parameter which is for steady flows defined as:

$$\theta' = \frac{\tau_b}{(\rho_s - \rho) g D_{50}}$$

Here τ_b is the shear stress at the bed in case of a smooth non moving bed and a logarithmic velocity profile.

In case the depth-averaged current velocity V is known:

$$\tau_b = \rho g \frac{V^2}{C'^2}$$

$$C' = 18 \log \left(\frac{12h}{k_s} \right)$$

C' is the Chézy coefficient, h is the water depth, and k_s is the roughness height.

If the a near-bed velocity at an arbitrary level $z = \delta$ ($u_b = u_b(\delta)$) is prescribed:

$$\tau_b = \frac{1}{2} \rho f_c' u_b^2$$

where f_c' is a friction factor here chosen as

$$f_c' = 2 \left(\frac{0.4}{\ln \frac{\delta}{z_0}} \right)$$

$$z_0 = \frac{k_s}{30}$$

The latter has a more general validity, as a logarithmic velocity profile is only assumed close to the bed. For both cases

$$k_s = \max\{3D_{90}, D_{50}[1 + 6(\theta - 1)]\}$$

A fit through a large number of data points yields the following best fit:

$$m = 10.4, n = 1.67$$

Summary transport formulae for steady flow

The transport formulae for steady flow of Wilson [39] and Ribberink [31] were discussed. The main differences are

- the model of Wilson is derived based on theoretical considerations, while the model of Ribberink is an empirical formula
- the shear stress is calculated over the whole sheet flow layer in the case of Wilson, while Ribberink uses the bed shear stress τ_b
- Ribberink included the critical Shields parameter for sediment motion in the transport formula

Apart from these differences, the formulae are very much alike:

$$\begin{aligned} q_s &= f_W(g, \rho_s, \rho)\tau^{1.5} && (Wilson) \\ q_s &= f_R(g, \rho_s, \rho, D_{50})(\theta' - \theta_{cr})^{1.67} && (Ribberink) \end{aligned}$$

where $\theta' \propto \tau_b$, and f_W and f_R are functions given by Wilson and Ribberink respectively.

A.1.2 Quasi steady oscillatory flow models

Ribberink and Al-Salem (1994)

Ribberink and Al Salem [32] describe three transport formulae in their paper. These are summarised below.

Madsen and Grant (1976)

$$\frac{q_s(t)}{w_s D_{50}} = 40\theta'(t)^3 \tag{A.3}$$

$$\theta'(t) = \frac{\frac{1}{2} f_w \left|U(t)\right| U(t)}{\Delta g D_{50}}$$

Bailard (1981):

$$q_s(t) = q_{s,b}(t) + q_{s,s}(t) \tag{A.4}$$

$$q_{s,b}(t) = \frac{\frac{1}{2} f_w \epsilon_b}{\Delta g \tan\phi} U_0^3(t)$$

$$q_{s,s}(t) = \frac{\frac{1}{2} f_w \epsilon_s}{\Delta g w_s} \left|U_0^3(t)\right| U_0(t)$$

Ribberink (1998)

The quasi-steady model for pure oscillatory flow proposed by Ribberink is the following:

$$\Phi_b(t) = \begin{cases} m(|\theta'(t)| - \theta_{cr})^n \frac{\theta'(t)}{|\theta'(t)|} & |\theta'| \geq \theta_{cr} \\ 0 & |\theta'| \geq \theta_{cr} \end{cases} \tag{A.5}$$

For oscillatory flow

$$\theta'(t) = \frac{\frac{1}{2}\rho f'_w \left|u_b(t)\right| u_b(t)}{(\rho_s - \rho) g D_{50}}$$

$$f'_w = \begin{cases} \exp\left(5.2\left(\frac{k_s}{\hat{a}}\right)^{0.194} - 5.98\right) & \frac{k_s}{\hat{a}} < 0.63 \\ 0.3 & \frac{k_s}{\hat{a}} \geq 0.63 \end{cases}$$

$$k_s = \max\{3D_{90}, D_{50}[1 + 6(\langle|\theta|\rangle - 1)]\}$$

$$\langle|\theta|\rangle = \frac{\langle|\tau_b(t)|\rangle}{(\rho_s - \rho) g D_{50}}$$

$$\langle|\tau_b(t)|\rangle = \frac{1}{2}\rho f'_w \langle u_b(t)^2\rangle = \frac{1}{4}\rho f'_w \hat{U}^2$$

In these formulae $u_b(t)$ is the time-dependent horizontal orbital velocity at $z = \delta$, f'_w is the wave friction factor (here the formula of Swart (1974) is used, which is based on Jonsson (1966)). $\hat{a}$ is the amplitude of the horizontal near-bed orbital flow, and $\hat{U}$ is the velocity amplitude of the oscillatory flow. Time-averaging (over half or full cycle) for net transport rates gives:

$$\langle\Phi_b(t)\rangle = m\langle(|\theta'(t)| - \theta_{cr})^n \frac{\theta'(t)}{|\theta'(t)|}\rangle \tag{A.6}$$

A fit through a large number of data points yields the following best fit:

$$m = 11, n = 1.65$$

For oscillatory flow with a superimposed current under an arbitrary angle Ribberink proposes

$$\langle\boldsymbol{\Phi}_b(t)\rangle = m\langle(|\theta'(t)| - \theta_{cr})^n \frac{\boldsymbol{\theta}'(t)}{|\theta'(t)|}\rangle \tag{A.7}$$

$$|\theta'(t)| = \sqrt{\theta'_x(t)^2 + \theta'_y(t)^2}$$

$$m = 11, n = 1.65$$

$$\boldsymbol{\theta}'(t) = \frac{\boldsymbol{\tau}_b(t)}{(\rho_s - \rho)gD_{50}} = \frac{\frac{1}{2}\rho f'_{cw} |u_b(t)| \, \mathbf{u}_b(t)}{(\rho_s - \rho)gD_{50}}$$

$$|u_b(t)| = \sqrt{u_{bx}^2(t) + u_{by}^2(t)}$$

$$\mathbf{u}_b(t) = \langle \mathbf{u}_b \rangle + \mathbf{u}_{b,osc}(t)$$

$$f'_{cw} = \alpha f'_c + (1 - \alpha) f'_w$$

$$\alpha = \frac{\langle u_b \rangle}{\langle u_b \rangle + \hat{U}_0}$$

Furthermore, for combined waves and currents the time-averaged bed shear stress, necessary for the roughness height, becomes for large values of the Shields parameter:

$$\langle |\tau_b| \rangle = \frac{1}{2}\rho f'_c \langle u_b \rangle^2 + \frac{1}{4}\rho f'_w \hat{U}_0^{\,2}$$

The suggestion that f'_{cw} is a linear combination of the wave and current friction factors was made by Madsen and Grant (1976).

Summary quasi steady transport formulae for oscillatory flow

The models of Madsen and Grant, Bailard, and Ribberink [31] were discussed. All of these models are empirical. Two profound differences can be distinguished between the models:

- Madsen and Grant and Ribberink do not distinguish between bed load and suspended load, while Bailard does this explicitly
- Ribberink included the critical Shields parameter for sediment motion in

his formula

The models can best be compared by writing them in the following forms:

$$q_s = f_{MG}(g, \rho_s, \rho, D_{50}, w_s, f_w)\,|U^5(t)|\,U(t) \qquad (Madson/Grant)$$

$$q_s = f_{B1}(g, \rho_s, \rho, f_w, \epsilon_b, \phi)U^3(t) + f_{B2}(g, \rho_s, \rho, w_s, f_w, \epsilon_s)\,|U^3(t)|\,U(t) \qquad (Bailard)$$

$$q_s = f_R(g, \rho_s, \rho, D_{50}, f_w)(|\theta'| - \theta_{cr})^{1.65} f(\theta') \qquad (Ribberink)$$

where $\theta' \propto U^2(t)$ and $f(\theta')$ is the normalised Shields parameter $\theta'(t)/|\theta'(t)|$.

A.1.3 Semi-unsteady oscillatory flow models

Dohmen-Janssen (1999)

Dohmen-Janssen [10] described the semi-unsteady model of Dibajnia and Watanabe (1992) and also proposed a new semi-unsteady model.

Dibajnia and Watanabe (1992)

$$\langle q_s \rangle = 0.001 w_s D_{50}\,|\Gamma|^{0.55}\,\frac{\Gamma}{|\Gamma|} \tag{A.8}$$

$$\Gamma = \frac{u_c T_c(\Omega_c^3 + \Omega_t'^3) - u_t T_t(\Omega_t^3 + \Omega_c'^3)}{(u_c + u_t)T}$$

$$u_i^2 = \tfrac{2}{T_i}\int_0^{T_i} u^2(t)dt \quad (i = c, t)$$

where Ω_c is the amount of sand entrained and transported during the positive half wave cycle, and Ω_t' is the amount of sand that is entrained during the negative half wave cycle, but transported during the positive half wave cycle because it has not resettled in time. Ω_c' and Ω_t are exactly the equivalent values for the transport during the negative half wave cycle.

Dohmen-Janssen [10] also proposed a new semi-unsteady model based on the quasi steady model of Ribberink [31]:

$$\langle q_s \rangle = r * \langle q_s \rangle_{Rib} \tag{A.9}$$

$$r = \frac{\langle q_{s,r} \rangle}{\langle q_{s,eq} \rangle} = \frac{\left(\frac{u_0}{u_1}\right)^2 + \frac{1}{2} + G(p)}{\left(\frac{u_0}{u_1}\right)^2 + \frac{3}{2}}$$

$$G(p) = \frac{P\cos\phi + Q\sin\phi}{(P^2+Q^2)^{3/2}}$$

$$P = \frac{1}{2} + \left[\frac{1}{16} + p^2\right]^{1/4} \cos\left(\frac{1}{2}\alpha\right)$$

$$Q = \left[\frac{1}{16} + p^2\right]^{1/4} \sin\left(\frac{1}{2}\alpha\right)$$

$$\alpha = \arctan(4p)$$

$$\phi = \arctan\left(-\frac{Q}{P}\right)$$

$$p = \frac{\epsilon_s \omega}{w_s^2} = \frac{\delta_s \omega}{w_s} = \frac{10\theta_w D_{50}\omega}{w_s} = \frac{5 f_w u_a^2 \omega}{(s-1)g w_s}$$

$$\begin{cases} q_{s,r}(t) = u_\infty(t) * \int_0^{z_\infty} C_r(z,t)dz \\ q_{s,eq}(t) = u_\infty(t) * \int_0^{z_\infty} C_{eq}(z,t)dz \end{cases}$$

p is the phase-lag parameter. The real sediment concentration C_r and the equilibrium sediment concentration C_{eq} are found by using the convection-diffusion equation for sediment:

$$\frac{\partial C}{\partial t} = \frac{\partial}{\partial z}\left[w_s C + \epsilon_s \frac{\partial C}{\partial z}\right] \tag{A.10}$$

For C_{eq}, set $\frac{\partial C}{\partial t} = 0$.

Summary semi-unsteady transport formulae for oscillatory flow

Two semi unsteady transport formulae for oscillatory flow were found in literature. The first is the model of Dibajnia and Watanabe and the second the model of Dohmen-Janssen [10]. The models are, contrary to the previous models, very different. In the model of Dibajnia and Watanabe the transport in the 'crest half wave cycle' and the 'trough half wave cycle' are calculated independently to account for phase lag effects, while Dohmen-Janssen modified the quasi steady model of Ribberink [31] by an unsteadiness parameter which is defined as the ratio between the sediment transport with and without phase lag effects.

A.2 RANS models

Several Reynolds Averaged Navier Stokes (RANS) models are proposed in literature for steady flow as well as oscillatory flow. They can be divided into advection-diffusion models and the more elaborate two-phase flow models. In this section we will discuss the models of Ribberink and Al-Salem [33], Davies and Li [8], and Guizien *et al.* [18] as the advection-diffusion models. One two-phase flow model for steady flow is mentioned in literature, being the model of Lamberti *et al* [22]. In the last section two-phase flow models for oscillatory flow are discussed, respectively Asano [1], Dong and Zhang [13], and Liu and Sato [25]. Hsu *et al.* [21] proposed a model for 'collisional sheet flow' of massive particles, i.e. the particles are supported by their collisional interactions rather than by turbulent velocity fluctuations in the fluid. This kind of model is only valid if the fall velocity of the particles exceeds the friction velocity of the fluid flow ($w_s/u^* > 1$). As they state in their concluding remarks, the model needs

to be extended for the case of sand in water as this case is not likely to satisfy the aforementioned conditions. Therefore, this model type is not included in this review.

A.2.1 Oscillatory advection-diffusion models

The advection-diffusion models for oscillatory sheet flow in literature are all based on the following set of equations:

$$\frac{\partial u}{\partial t} = -\frac{1}{\rho}\frac{\partial p}{\partial x} + \frac{\partial}{\partial z}\left(\nu_e \frac{\partial u}{\partial z}\right) \tag{A.11}$$

$$\frac{\partial C}{\partial t} = \frac{\partial}{\partial z}\left(w_s C + \epsilon_s \frac{\partial C}{\partial z}\right) \tag{A.12}$$

The models mainly differ in their specific turbulence closure schemes and in some cases the boundary conditions are a little different. In the following subsections the turbulence closures and boundary conditions of three advection-diffusion models for oscillatory sheet flow will be discussed. The first is the model of Ribberink and Al-Salem [33], in which the turbulence closure is based on Prandtl's mixing length theory and a reference concentration type boundary conditions is applied on the lower boundary. In the second subsection the model of Davies and Li [8] is described, which has a one-equation turbulence closure and reference concentration as well as pick-up function-boundary conditions. Finally we will discuss the model of Guizien *et al.* [18], in which a two-equation turbulence closure is chosen and reference concentration boundary conditions.

Ribberink and Al-Salem (1995)

Ribberink and Al-Salem [33] use the Prandtl mixing length theory to form a turbulence closure:

$$\nu_e = l_m^2 \left|\frac{\partial u}{\partial z}\right| = (\kappa z)^2 \left|\frac{\partial u}{\partial z}\right|$$

and

$$\epsilon_s = \nu_e$$

The horizontal pressure gradient in this model is simply related to the free stream velocity:

$$\frac{\partial p}{\partial x} = -\rho \frac{\partial U_0}{\partial t}$$

Lower boundary conditions:

$$\begin{aligned} &at \quad z = z_0 = k_s/30 = 2.5D_{50}/30 : \quad u = 0 \\ &at \quad z = z_a = 2D_{50} : \qquad \begin{cases} C = C(z_a, t) \\ or \\ \frac{\partial C}{\partial z} = f(\tau_b(t), G) \end{cases} \end{aligned}$$

where G is a set of sediment parameters.

Upper boundary conditions:

$$\begin{aligned} &at \quad z = z_{up} : \quad u = U_0 \\ &at \quad z = z_{up} : \quad \frac{\partial C}{\partial z} = 0 \end{aligned}$$

Davies and Li (1997)

Davies and Li [8] choose a one-equation turbulence closure for the turbulent kinetic energy k, while the vertical mixing length scale l_m is based von

Karman's similarity hypothesis:

$$\nu_e = c_1 l_m k^{1/2}$$

$$\epsilon_s = \nu_e$$

$$\frac{\partial k}{\partial t} = \nu_e \left(\frac{\partial u}{\partial z}\right)^2 + \epsilon_s \frac{g}{\rho}\frac{\partial \rho_m}{\partial z} - \frac{c_2 k^{3/2}}{l} + \frac{\partial}{\partial z}\left(\epsilon_k \frac{\partial k}{\partial z}\right)$$

$$l_m = \kappa \left(1 - \frac{z}{h}\right)^{1/2} k^{1/2} \left(\int_{z_0}^{z} k^{-1/2} dz + z_0 k_0^{-1/2}\right)$$

where $\rho_m = \rho_s C + \rho(1 - C)$ and c_1 is a constant.

Furthermore

$$-\frac{1}{\rho}\frac{\partial p}{\partial x} = -\frac{1}{\rho}\frac{\partial \bar{P}}{\partial x} + \frac{\partial U_0}{\partial t}$$

where the first term on the right hand site is a pressure gradient generating a mean current, while the second term is related to the oscillatory flow.

Lower boundary conditions:

$$\begin{aligned} &at \quad z = z_0 = k_s/30 = 2.5D_{50}/30 : \quad && u = 0 \\ &at \quad z = z_a = 2D_{50} : && C = C_b \\ &at \quad z = z_{bottom} : && \tfrac{\partial k}{\partial z} = 0 \end{aligned}$$

where

$$C_b = \frac{0.65}{(1 + 1/\lambda)^3}$$

where λ is the linear concentration given by

$$\begin{cases} \lambda = \left(\frac{|\theta| - \theta_c - \pi p_*/6}{0.027|\theta| s}\right)^{1/2} & for \quad |\theta| > \theta_c + \pi p_*/6 \\ \lambda = 0 & for \quad |\theta| \leq \theta_c + \pi p_*/6 \end{cases}$$

where

$$p_* = \left[1 + \left(\frac{\pi/6}{|\theta| - \theta_c}\right)^4\right]^{-1/4}$$

Upper boundary conditions:

$$\begin{aligned} at \quad z = h: \quad & \nu_e \tfrac{\partial u}{\partial z} = 0 \\ at \quad z = h: \quad & \tfrac{\partial C}{\partial z} = 0 \\ at \quad z = z_{up}: \quad & \tfrac{\partial k}{\partial z} = 0 \end{aligned}$$

Guizien *et al.* (2003)

Guizien *et al.* [18] use a slightly modified version of the momentum equation for the fluid (Eq. A.11), in the sense that not only the turbulent eddy viscosity is included in the equation but also the kinematic viscosity of water:

$$\frac{\partial u}{\partial t} = -\frac{1}{\rho}\frac{\partial p}{\partial x} + \frac{\partial}{\partial z}\left((\nu + \nu_e)\frac{\partial u}{\partial z}\right) \tag{A.13}$$

For the turbulence closure they used a two-equation scheme with one equation for the turbulent kinetic energy k and one for the energy dissipation rate ω:

$$\nu_e = \alpha^* \tfrac{k}{\omega} \tfrac{1 - C_3\Omega}{(1 - C_1\Omega)(1 - C_2\Omega)} \quad (\Omega = 2\tfrac{g}{\rho}\tfrac{d\rho_m}{dz}\tfrac{4}{\omega^2})$$

$$\epsilon_s = \nu_e \frac{1 - C_2\Omega}{1 - C_3\Omega}$$

where C_1, C_2, and C_3 are coupling constants.

$$\frac{\partial k}{\partial t} = \nu_e \left(\frac{\partial u}{\partial z}\right)^2 + \epsilon_s \frac{g}{\rho}\frac{\partial \rho_m}{\partial z} - \beta^* k\omega + \frac{\partial}{\partial z}\left[(\nu + \sigma\nu_e)\frac{\partial k}{\partial z}\right]$$

$$\frac{\partial \omega}{\partial t} = \alpha\nu_e \frac{\omega}{k}\left(\frac{\partial u}{\partial z}\right)^2 - \beta\omega^2 + \frac{\partial}{\partial z}\left((\nu + \sigma\nu_e)\frac{\partial \omega}{\partial z}\right) + c_0 \frac{\omega}{2k\rho}\epsilon_s \frac{\partial \rho_m}{\partial z}$$

$$\alpha^* = \frac{\alpha_0^* + Re_T/R_K}{1 + Re_T/R_K}$$
$$\alpha = \frac{13}{25}\frac{\alpha_0 + Re_T/R_\omega}{1 - Re_T/R_\omega}(\alpha^*)^{-1}$$
$$\beta^* = \frac{9}{100}\frac{4/15 + (Re_T/R_\beta)^4}{1 + (Re_T/R_\beta)4}$$

where $Re_T = \frac{k}{\nu\omega}$, $\beta = \beta_0 = \frac{9}{125}$, $\alpha_0^* = \frac{\beta_0}{3}$, $\alpha_0 = \frac{1}{9}$, $R_\beta = 2.95$, and $c_0 = 0.8$. Unfortunately, σ, σ^*, R_K, and R_β cannot be estimated through a simple argument.

The pressure gradient is defined as in the model of Davies and Li [8]:

$$-\frac{1}{\rho}\frac{\partial p}{\partial x} = -\frac{1}{\rho}\frac{\partial \bar{P}}{\partial x} + \frac{\partial U_0}{\partial t}$$

Lower boundary conditions

$$\begin{aligned} at \quad z = 0: \quad & u = 0 \\ at \quad z = z_a = 2D_{50}: \quad & C = \max(C_a, C_b) \\ at \quad z = 0: \quad & k = 0 \\ at \quad z = 0: \quad & \omega_{wall}\frac{u^{*2}}{\nu}S_R \end{aligned}$$

where $S_R = (50/k_N^+)^2$ if $k_N^+ < 25$, and $S_R = 100/k_N^+$ if $k_N^+ \geq 25$. C_a is a reference concentration and C_b results from settling particles.

Upper boundary conditions

$$\begin{aligned} at \quad z = z_h: \quad & u = U_0 \\ at \quad z = z_h: \quad & \frac{\partial C}{\partial z} = 0 \\ at \quad z = z_h: \quad & \frac{\partial k}{\partial z} = 0 \\ at \quad z = z_h: \quad & \frac{\partial \omega}{\partial z} = 0 \end{aligned}$$

Summary advection-diffusion models for oscillatory sheet flow

Three advection-diffusion models for oscillatory sheet flow were discussed. In increasing order of complexity these are the model of Ribberink and Al-Salem [33], Davies and Li [8], and Guizien *et al.* [18].All of these models are based on the following set of equations:

$$\frac{\partial u}{\partial t} = -\frac{1}{\rho}\frac{\partial p}{\partial x} + \frac{\partial}{\partial z}\left(\nu_e \frac{\partial u}{\partial z}\right)$$

$$\frac{\partial C}{\partial t} = \frac{\partial}{\partial z}\left(w_s C + \epsilon_s \frac{\partial C}{\partial z}\right)$$

The turbulence closure in the model of Ribberink and Al-Salem is based on Prandtl's mixing length theory where the mixing length is simply chosen as κz, and the assumption that $\epsilon_s = \nu_e$. Davies and Li used a slightly more sophisticated closure by imposing a one-equation scheme (the equation being the differential equation for the turbulent kinetic energy k), while the mixing length is calculated using von Karman's similarity hypothesis. Furthermore, like Ribberink and Al-Salem Davies and Li also assume $\epsilon_s = \nu_e$. Guizien *et al.* use a two-equation turbulence closure scheme, with one differential equation for k and one for the energy dissipation rate ω.

The horizontal pressure gradient is in all three models directly related to the free stream velocity U_0 by the following relation:

$$\frac{\partial p}{\partial x} = -\rho \frac{\partial U_0}{\partial t}$$

Davies and Li [8] and Guizien *et al.* [18] also included a pressure gradient generating a mean current.

As the pick-up function boundary conditions in the model of Davies and Li did not show a significant improvement, the differences in the boundary conditions are considered to be of only minor importance.

A.2.2 Steady two-phase flow models

Lamberti *et al.* (1990)

Lamberti *et al.* [22] made a two-phase model for steady flow over a sloping bed. Velocity and pressure are here independent of x, z, and t. The coordinate system used by Lamberti *et al.* [22] is schematically given in Figure A.2.

The governing equations are then as follows:

$$(1 - C)w + Cw_s = 0 \tag{A.14}$$

$$Cw_s - \epsilon_s \frac{C}{z} = 0 \tag{A.15}$$

$$\frac{\partial \tau_f}{\partial z} + \rho g \sin\alpha - f_x = 0 \tag{A.16}$$

$$\frac{\partial \sigma_f}{\partial z} + \rho g \cos\alpha + f_z = 0 \tag{A.17}$$

$$\frac{\partial \tau_s}{\partial z} + (\rho_s - \rho) C g \sin\alpha + f_x = 0 \tag{A.18}$$

$$\frac{\partial \sigma_s}{\partial z} + (\rho_s - \rho) C g \cos\alpha - f_z = 0 \tag{A.19}$$

where τ_f and σ_f are the fluid shear and normal stresses respectively, and τ_s and σ_s are the sediment shear and normal stresses respectively. α is the bed slope.

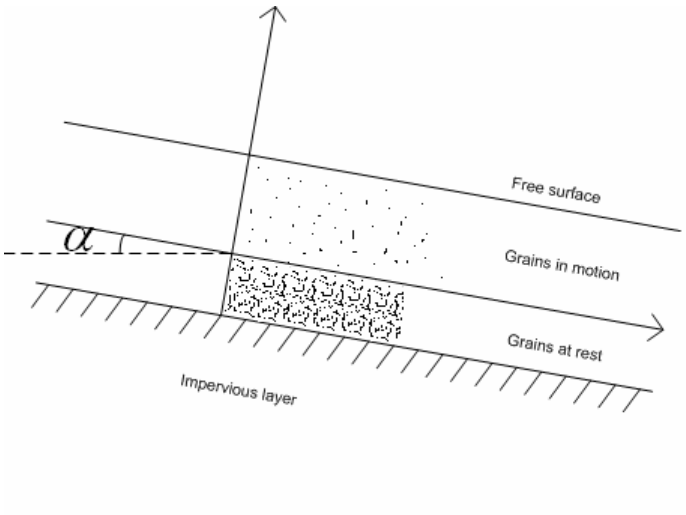

Figure A.2: Coordinate system used by Lamberti et al. Source: Lamberti et al [22]

The model is closed by the following constitutive equations:

$$\tau_f = \rho(1-C)l_m^2\left(\frac{\partial u}{\partial z}\right)^2 \tag{A.20}$$

$$\tau_s = [f_{\tau k}(C) + f_{\tau C}(C)]\rho_s D^2\left(\frac{\partial u_s}{\partial z}\right)^2 \tag{A.21}$$

$$\sigma_s = [f_{\sigma k}(C) + f_{\sigma C}(C)]\rho_s D^2 \left(\frac{\partial u_s}{\partial z}\right)^2 \tag{A.22}$$

where l_m is Prandtl's mixing length, and $f_{\tau k}(C)$, $f_{\tau C}(C)$, $f_{\sigma k}(C)$, and $f_{\sigma C}(C)$ are parameters given by Babic and Shen (1989).

Furthermore, the interaction forces consists of buoyancy and drag forces in this model. They are therefore defined as:

$$f_x = \frac{3}{4D}\rho C C_D \sqrt{u_r^2 + w_r^2} u_r \tag{A.23}$$

$$f_z = \frac{3}{4D}\rho C C_D \sqrt{u_r^2 + w_r^2} w_r + \rho C g \tag{A.24}$$

where C_D is the drag coefficient and u_r and w_r are the relative velocities between the fluid and solid phase in horizontal and vertical direction respectively.

A.2.3 Oscillatory two-phase flow models

All two-phase flow models for oscillatory sheet flow in literature are based on the same set of equations, but differ in the simplifications made and choice and specific form of the constitutive equations. The basis for these models is given by Eq. A.25 to Eq. A.28. Eq. A.25 is the mass balance for the fluid phase, Eq. A.26 is the mass balance for the solid phase, and Eq. A.27 and Eq. A.28 are the momentum balances for the fluid and solid phase respectively.

$$\frac{\partial \rho(1-C)}{\partial t} + \frac{\partial \rho(1-C)u_j}{\partial x_j} = 0 \tag{A.25}$$

$$\frac{\partial \rho_s C}{\partial t} + \frac{\partial \rho_s C u_{s,j}}{\partial x_j} = 0 \tag{A.26}$$

$$\frac{\partial \rho(1-C)u_i}{\partial t} + \frac{\partial \rho(1-C)u_i u_j}{\partial x_j} = -(1-C)\frac{\partial p}{\partial x_i} - \rho(1-C)g\delta_{i2} - f_i \quad \text{(A.27)}$$

$$\frac{\partial \rho_s C u_{s,i}}{\partial t} + \frac{\partial \rho_s C u_{s,i} u_{s,j}}{\partial x_j} = -C\frac{\partial p}{\partial x_i} - \rho_s C g\delta_{i2} + \frac{\partial T_{s,ij}}{\partial x_j} + f_i \quad \text{(A.28)}$$

where ρ and ρ_s are the density of water and sand respectively, C is the sediment concentration, p is the fluid pressure, g is the acceleration due to gravity, δ_{ij} is the Kronecker delta, f_i is the total interaction force between the fluid and solid phase, $T_{s,ij}$ is the intergranular stress tensor, t is time, and u_j and $u_{s,j}$ are the fluid and solid velocities in the x_j direction respectively.

Eq. A.25 to A.28 contain turbulent quantities. Reynolds averaging gives (the full derivation given in Appendix B):

$$\frac{\partial \rho(1-C)}{\partial t} + \frac{\partial \rho(1-C)u_j}{\partial x_j} = \frac{\partial \phi_j^m}{\partial x_j} \quad \text{(A.29)}$$

$$\frac{\partial \rho_s C}{\partial t} + \frac{\partial \rho_s C u_{s,j}}{\partial x_j} = \frac{\partial \phi_{s,j}^{s,m}}{\partial x_j} \quad \text{(A.30)}$$

$$\frac{\partial \rho(1-C)u_i}{\partial t} + \frac{\partial \rho(1-C)u_i u_j}{\partial x_j} = -(1-C)\frac{\partial p}{\partial x_i} - \rho(1-C)g\delta_{i2} + \frac{\partial \phi_i^a}{\partial t} + \frac{\partial \tau_{ij}^c}{\partial x_j} - f_i \quad \text{(A.31)}$$

$$\frac{\partial \rho_s C u_{s,i}}{\partial t} + \frac{\partial \rho_s C u_{s,i} u_{s,j}}{\partial x_j} = -C\frac{\partial p}{\partial x_i} - \rho_s C g\delta_{i2} + \frac{\partial \phi_{s,i}^{s,a}}{\partial t} + \frac{\partial \tau_{s,ij}^{s,c}}{\partial x_j} + \frac{\partial T_{s,ij}}{\partial x_j} + f_i \quad \text{(A.32)}$$

ϕ_i^a and $\phi_{s,i}^a$ represent the turbulent fluxes related to the acceleration term of the fluid and solid phase respectively, and ϕ_i^c and $\phi_{s,i}^c$ are the turbulent fluxes related to the convective terms.

Asano (1990)

Asano [1] is mentioned in almost every text on sheet flow modelling. He was, to the authors knowledge, the first to derive a full two-phase flow model

for oscillatory sheet flow. He performed some quite rigourous simplifications to be able to solve the system of equations, as he effectively replaced the whole vertical momentum balances by simplified equations.

The following constitutive equation are implemented:

$$\overline{C'w'} \simeq \overline{C'w'_s} = -\epsilon_s \frac{\partial C}{\partial z} \tag{A.33}$$

$$\overline{u'_s w'_s} \simeq \overline{u'w'} = -\nu_e \frac{\partial u}{\partial z} \tag{A.34}$$

According to Asano, the interaction force consists of a drag and a buoyancy part:

$$f_x = \frac{3}{4D}\rho C C_D |u_r| u_r \tag{A.35}$$

$$f_z = \frac{3}{4D}\rho C C_D \sqrt{u_r^2 + w_r^2} w_r + \rho C g \tag{A.36}$$

Asano assumes $u \gg w$, $u_s \gg w_s$, and $u\overline{C'w'} \gg \overline{u'C'w'}$. The turbulent stress tensor is then

$$\tau^c_{xz} = \rho \left\{(1-C)u'w' - uC'w'\right\} = \rho \left\{(1-C)\nu_e \frac{\partial u}{\partial z} - u\epsilon_s \frac{\partial C}{\partial z}\right\} \tag{A.37}$$

The turbulent stresses in the solid phase are described in a similar way as in the fluid phase:

$$\tau^c_{s,xz} = \rho_s \left\{C u'_s w'_s - u_s C' w'_s\right\} = \rho_s \left\{C\nu_e \frac{\partial u_s}{\partial z} - u_s \epsilon_s \frac{\partial C}{\partial z}\right\} \tag{A.38}$$

and for the intergranular stress tensor the constitutive equation of Savage-McKeown is adopted:

$$T_{s,xz} = 1.2\lambda^2 \rho \nu \frac{\partial u_s}{\partial z} \tag{A.39}$$

Finally, the vertical velocity of the solid phase and the pressure gradient are not derived from the governing equations, but imposed as follows:

$$w_s = w_{f0}\left[1 - \frac{C}{C_m}\right]^n \quad (n = 2.3) \tag{A.40}$$

$$\frac{\partial p}{\partial x} = -\rho\frac{\partial U_0}{\partial t} \tag{A.41}$$

Dong and Zhang (1999)

Dong and Zhang [13] built a comprehensive two-phase flow model. The most important assumption in this model is that convective terms are neglected.

The constitutive equations are the following. The interaction force f_i consist of drag, lift, and added mass, described by these formulae:

$$f_x = \frac{3}{4D}\rho C C_D\sqrt{u_r^2 + w_r^2}u_r + \rho C C_M\frac{du_r}{dt} \tag{A.42}$$

$$f_z = \frac{3}{4D}\rho C C_D\sqrt{u_r^2 + w_r^2}w_r + \rho C C_M\frac{dw_r}{dt} + \frac{3}{4}\rho C C_L\left|u_r\right|\frac{du_r}{dt} \tag{A.43}$$

where u_r and w_r are the relative velocities between the solid and fluid phase, $C_L = 4/3$ is the lift coefficient, $C_M = 1/2$ is the added mass coefficient, and the drag coefficient C_D is calculated by Rubey's law:

$$C_D = \frac{24}{Re} + 2 = \frac{24\nu}{D\sqrt{u_r^2 + w_r^2}} + 2$$

where ν is the kinematic viscosity of water and D the sediment particle diameter.

The intergranular stress tensors $T_{s,xz}$ and $T_{s,zz}$ are described by the formu-

lae:

$$T_{s,xz} = 1.2\lambda^2 \rho\nu \frac{\partial u_s}{\partial z} \tag{A.44}$$

$$T_{s,zz} = 1.2\lambda^2 \rho\nu \frac{\partial u_s}{\partial z} \cot\phi \tag{A.45}$$

where ϕ is the dynamic friction angle of the sediment, and λ is the linear concentration as it was proposed by Bagnold [2]:

$$\lambda = \frac{1}{[(C_m/C)^{1/3} - 1]}$$

where C_m is the theoretical maximum concentration. Note that the turbulent stresses in the solid phase as a result of Reynolds averaging of the advective term is not included because advection is neglected.

Although advection is neglected, the turbulent stress in the fluid phase is included anyway. The turbulent stresses in the vertical direction τ_{zz} are neglected, while the horizontal stresses are calculated based on Prandtl's mixing length theory:

$$\tau_{xz}^c = \rho(1-C) l^2 \left|\frac{\partial u_m}{\partial z}\right| \frac{\partial u_m}{\partial z} \tag{A.46}$$

where l is the mixing length given by

$$l = \kappa \int_{-\infty}^{z} \frac{C_m - C}{C_m} dz$$

and u_m is the concentration weighted velocity given by:

$$u_m = (1-C)u + Cu_s$$

For the time-averaged fluctuations a mixing coefficient is introduced:

$$\overline{C'w'_s} = \overline{C'w'} = -\epsilon_s \frac{\partial C}{\partial z} \tag{A.47}$$

where they use the following expression for the mixing coefficient ϵ_s:

$$\epsilon_s = \left[\left(1 - \frac{C}{C_m}\right) l\right]^2 \left|\frac{\partial u_m}{\partial z}\right| + 5\nu$$

Finally, the horizontal pressure gradient is simply related to the free stream velocity in the wave U_0:

$$\frac{\partial p}{\partial x} = -\rho \frac{dU_0}{dt} \tag{A.48}$$

Liu and Sato (2005)

The model of Liu and Sato [25] is, to a large extent, based on the model of Dong and Zhang [13]. As the two models are very similar, only the differences will be addressed in this section.

Liu and Sato [25] claim that the value of ϵ_s will suddenly drop around the overshoot height in the expression of Dong and Zhang [14], and therefore propose a different relation:

$$\epsilon_s = \max\left(\alpha_b D_* \hat{U}_0 \delta_s, A\phi\nu_e\right)$$

where $\alpha_b = 0.0005$ is a coefficient, $D_* = d\left[(s-1)g/\nu^2\right]^{1/3}$ is the dimensionless grain size, U is the free stream velocity amplitude, and δ_s is the sheet flow layer thickness (based on the 8 volume-percentage criterion). $A = 0.5{+}1.5\left(w_s/u^*\right)^{0.5}$ describes the difference in the diffusion of a fluid particle and a sediment particle, $\phi = 1 + (C/C_m)^{0.5} - 2(C/C_m)^{0.25}$ is a measure for the influence of sediment

particles on the turbulence structure of the fluid, and ν_e is the turbulent eddy viscosity, here defined as:

$$\nu_e = \begin{cases} 0 & z_b \leq z < z|_{u_s=0} \\ (1-C)\kappa u_* z(1-\frac{z}{h}) & z|_{u_s=0} \leq z \leq z|_{\nu_e=(\nu_e)_{max}} \\ (\nu_e)_{max} & z_{\nu_e=(\nu_e)_{max}} < z \leq z_u \end{cases}$$

For the pressure gradient they use a more complicated expression, which also includes a pressure gradient p_c to generate a steady current and a concentration related damping factor:

$$\frac{\partial p}{\partial x} = -\rho \left(\frac{dU_0}{dt} + p_c \right) \left(1 - \left(\frac{C}{C_m} \right)^6 \right) \tag{A.49}$$

Summary two-phase models for oscillatory sheet flow

In this section three two-phase flow models for oscillatory sheet flow were discussed. In chronological order these are the models of Asano [1], Dong and Zhang [13], and Liu and Sato [25]. The three models are based on the following set of Reynolds-averaged equations:

$$\frac{\partial \rho(1-C)}{\partial t} + \frac{\partial \rho(1-C)u_j}{\partial x_j} = \frac{\partial \phi_j^m}{\partial x_j}$$

$$\frac{\partial \rho_s C}{\partial t} + \frac{\partial \rho_s C u_{s,j}}{\partial x_j} = \frac{\partial \phi_{s,j}^{s,m}}{\partial x_j}$$

$$\frac{\partial \rho(1-C)u_i}{\partial t} + \frac{\partial \rho(1-C)u_i u_j}{\partial x_j} = -(1-C)\frac{\partial p}{\partial x_i} - \rho(1-C)g\delta_{i2} + \frac{\partial \phi_i^a}{\partial t} + \frac{\partial \tau_{ij}^c}{\partial x_j} - f_i$$

$$\frac{\partial \rho_s C u_{s,i}}{\partial t} + \frac{\partial \rho_s C u_{s,i} u_{s,j}}{\partial x_j} = -C\frac{\partial p}{\partial x_i} - \rho_s C g\delta_{i2} + \frac{\partial \phi_{s,i}^{s,a}}{\partial t} + \frac{\partial \tau_{s,ij}^{s,c}}{\partial x_j} + \frac{\partial T_{s,ij}}{\partial x_j} + f_i$$

All three models neglect the acceleration related turbulent fluxes ϕ_i^a and $\phi_{s,i}^{s,a}$. Furthermore some differences are found between the models:

- Dong and Zhang and Liu and Sato neglect advective terms. Asano includes these terms, but substitutes the vertical momentum balances by simpler equations in order to be able to solve the set of equations.
- Asano includes drag and buoyancy in the interaction force between the fluid and the solid phase, while Dong and Zhang and Liu and Sato include drag, lift, and added mass.
- Dong and Zhang relate the horizontal pressure difference only to the free stream velocity, while Liu and Sato also include a pressure gradient generating a steady current and a concentration related damping factor. Asano assumes a constant pressure difference throughout the boundary layer.
- Asano neglects the vertical turbulent intergranular stresses $tau_{s,zz}$ while Dong and Zhang and Liu and Sato take them into account.
- The choice of parametrisation differs from one model to another.

A.3 Discrete Particle Models

Although two existing DPM models for sediment transport were found by the author, none was suitable for sediment transport in sheet flow conditions for typically Dutch coastal sand. The model by Drake and Calantoni [15] is, like the model of Hsu *et al.* [21], made for collisional sheet flow, i.e. for relatively large particles. A major advantage of the assumption of collisional sheet flow

is that lubrication forces can be ignored. They validated their model with experiments with 1.1 mm sand, which is about an order of magnitude larger than the sediment size along the Dutch coast. Vittori [37] also published a DPM model for sediment transport under waves, but this model is only valid in dilute systems as only a one-way coupling is made.

Appendix B

Reynolds averaging in two-phase continuum models

In this Appendix the Reynolds-averaged equations are derived. First we discuss the mass balance of the fluid phase and solid phase respectively. The momentum balances are included in the second section.

B.0.1 Mass balance

Fluid phase

$$\frac{\partial \rho(1-C)}{\partial t} + \frac{\partial \rho(1-C)u_j}{\partial x_j} = 0 \tag{B.1}$$

Reynolds decomposition: $C = \bar{C} + C'$, $u_j = \bar{u_j} + u'_j$. ρ is not assumed to be a turbulent fluctuating quantity.

$$\frac{\partial \rho(1-\bar{C}-C')}{\partial t} + \frac{\partial \rho(1-\bar{C}-C')(\bar{u_j}+u'_j)}{\partial x_j} = 0$$

$$\frac{\partial(\rho(1-\bar{C})-\rho C')}{\partial t}+\frac{\partial\rho(\bar{u_j}+u'_j-\bar{C}\bar{u_j}-\bar{C}u'_j-C'\bar{u_j}-C'u'_j)}{\partial x_j}=0$$

Average over time:

$$\overline{\frac{\partial(\rho(1-\bar{C})-\rho C')}{\partial t}+\frac{\partial\rho(\bar{u_j}+u'_j-\bar{C}\bar{u_j}-\bar{C}u'_j-C'\bar{u_j}-C'u'_j)}{\partial x_j}}=\bar{0}$$

$$\overline{\frac{\partial(\rho(1-\bar{C})-\rho C')}{\partial t}}+\overline{\frac{\partial\rho(\bar{u_j}+u'_j-\bar{C}\bar{u_j}-\bar{C}u'_j-C'\bar{u_j}-C'u'_j)}{\partial x_j}}=0$$

$$\frac{\partial\overline{(\rho(1-\bar{C})-\rho C')}}{\partial t}+\frac{\partial\overline{(\rho\bar{u_j}+\rho u'_j-\rho\bar{C}\bar{u_j}-\rho\bar{C}u'_j-\rho C'\bar{u_j}-\rho C'u'_j)}}{\partial x_j}=0$$

$$\frac{\partial(\overline{\rho(1-\bar{C})}-\overline{\rho C'})}{\partial t}+\frac{\partial(\overline{\rho\bar{u_j}}+\overline{\rho u'_j}-\overline{\rho\bar{C}\bar{u_j}}-\overline{\rho\bar{C}u'_j}-\overline{\rho C'\bar{u_j}}-\overline{\rho C'u'_j})}{\partial x_j}=0$$

$$\frac{\partial(\rho(1-\bar{C})-\rho\overline{C'})}{\partial t}+\frac{\partial(\rho\bar{u_j}+\rho\overline{u'_j}-\rho\bar{C}\bar{u_j}-\rho\bar{C}\overline{u'_j}-\rho\bar{u_j}\overline{C'}-\rho\overline{C'u'_j})}{\partial x_j}=0$$

$$\frac{\partial\rho(1-\bar{C})}{\partial t}+\frac{\partial(\rho\bar{u_j}-\rho\bar{C}\bar{u_j}-\rho\overline{C'u'_j})}{\partial x_j}=0$$

$$\frac{\partial\rho(1-\bar{C})}{\partial t}+\frac{\partial\rho(1-\bar{C})\bar{u_j}}{\partial x_j}=\frac{\partial\rho\overline{C'u'_j}}{\partial x_j}$$

We will define the turbulent flux in the mass balance ϕ_j^m as

$$\phi_j^m=\rho\overline{C'u'_j}$$

The bars on non-fluctuation quantities can be left out for notational convenience. The complete mass balance for the fluid phase is then:

$$\frac{\partial\rho(1-C)}{\partial t}+\frac{\partial\rho(1-C)u_j}{\partial x_j}=\frac{\partial\phi_j^m}{\partial x_j} \tag{B.2}$$

Solid phase

We can derive the Reynolds averaged mass balance for the solid phase in an equivalent way:

$$\frac{\partial \rho_s C}{\partial t} + \frac{\partial \rho_s C u_{s,j}}{\partial x_j} = 0 \tag{B.3}$$

Reynolds decomposition: $C = \bar{C} + C'$, $u_{s,j} = \bar{u_{s,j}} + u'_{s,j}$. ρ_s is not assumed to be a turbulent fluctuating quantity.

$$\frac{\partial \rho_s(\bar{C} + C')}{\partial t} + \frac{\partial \rho_s(\bar{C} + C')(\bar{u}_{s,j} + u'_{s,j})}{\partial x_j} = 0$$

$$\frac{\partial(\rho_s\bar{C} + \rho_s C')}{\partial t} + \frac{\partial \rho_s(\bar{C}\bar{u}_{s,j} + \bar{C}u'_{s,j} + C'\bar{u}_{s,j} + C'u'_{s,j})}{\partial x_j} = 0$$

Average over time:

$$\overline{\frac{\partial(\rho_s\bar{C} + \rho_s C')}{\partial t}} + \overline{\frac{\partial \rho_s(\bar{C}\bar{u}_{s,j} + \bar{C}u'_{s,j} + C'\bar{u}_{s,j} + C'u'_{s,j})}{\partial x_j}} = \bar{0}$$

$$\frac{\partial\overline{(\rho_s\bar{C} + \rho_s C')}}{\partial t} + \frac{\partial\overline{(\rho_s\bar{C}\bar{u}_{s,j} + \rho_s\bar{C}u'_{s,j} + \rho_s C'\bar{u}_{s,j} + \rho_s C'u'_{s,j})}}{\partial x_j} = 0$$

$$\frac{\partial\overline{(\rho_s\bar{C}) + \rho_s C')}}{\partial t} + \frac{\partial\overline{(\rho_s\bar{C}\bar{u}_{s,j} + \rho_s\bar{C}u'_{s,j} + \rho_s C'\bar{u}_{s,j} + \rho_s C'u'_{s,j})}}{\partial x_j} = 0$$

$$\frac{\partial(\overline{\rho_s\bar{C}} + \overline{\rho_s C'})}{\partial t} + \frac{\partial(\overline{\rho_s\bar{C}\bar{u}_{s,j}} + \overline{\rho_s\bar{C}u'_{s,j}} + \overline{\rho_s C'\bar{u}_{s,j}} + \overline{\rho_s C'u'_{s,j}})}{\partial x_j} = 0$$

$$\frac{\partial(\rho_s\bar{C} + \rho\overline{C'})}{\partial t} + \frac{\partial(\rho_s\bar{C}\bar{u}_{s,j} + \rho_s\bar{C}\overline{u}'_{s,j} + \rho_s\bar{u}_{s,j}\overline{C'} + \rho_s\overline{C'u'_{s,j}})}{\partial x_j} = 0$$

$$\frac{\partial \rho_s\bar{C})}{\partial t} + \frac{\partial(\rho_s\bar{C}\bar{u}_{s,j} + \rho_s\overline{C'u'_{s,j}})}{\partial x_j} = 0$$

$$\frac{\partial \rho_s\bar{C}}{\partial t} + \frac{\partial \rho_s\bar{C}\bar{u}_{s,j}}{\partial x_j} = -\frac{\partial \rho_s\overline{C'u'_{s,j}}}{\partial x_j}$$

We will define the turbulent flux in the mass balance of the solid phase $\phi_{s,j}^{s,m}$ as

$$\phi_{s,j}^{s,m} = \rho_s \overline{C' u'_{s,j}}$$

The bars on non-fluctuation quantities can be left out for notational convenience. The complete mass balance for the solid phase is then:

$$\frac{\partial \rho_s C}{\partial t} + \frac{\partial \rho_s C u_{s,j}}{\partial x_j} = -\frac{\partial \phi_{s,j}^{s,m}}{\partial x_j} \tag{B.4}$$

B.0.2 Momentum balance

Fluid phase

$$\frac{\partial \rho(1-C)u_i}{\partial t} + \frac{\partial \rho(1-C)u_i u_j}{\partial x_j} = -(1-C)\frac{\partial p}{\partial x_i} - \rho(1-C)g\delta_{i2} - f_i \tag{B.5}$$

Reynolds decomposition: $C = \bar{C} + C'$, $u_i = \bar{u_i} + u'_i$, $u_j = \bar{u_j} + u'_j$. ρ and p and g are assumed not to be turbulent fluctuating quantities. Therefore, the right hand side terms will not generate Reynolds stresses, and we can thus focus on the first two terms. They are now treated separately. As shown in the previous section:

$$\frac{\partial \rho(1-C)u_i}{\partial t} = \frac{\partial \rho(1-\bar{C})\bar{u}_i}{\partial t} - \frac{\partial \rho \overline{C' u'_i}}{\partial t} \tag{B.6}$$

We will define the acceleration related turbulent flux ϕ_i^a as

$$\phi_i^a = \rho \overline{C' u'_i}$$

The second term is somewhat more involved:

$$\frac{\partial \rho(1-C)u_i u_j}{\partial x_j} = \frac{\partial \rho(1-\bar{C}-C')(\bar{u}_i+u_i')(\bar{u}_j+u_j')}{\partial x_j}$$

$$= \frac{\partial \rho(\bar{u}_i+u_i'-\bar{C}\bar{u}_i-\bar{C}u_i'-C'\bar{u}_i-C'u_i')(\bar{u}_j+u_j')}{\partial x_j}$$

$$= \frac{\partial}{\partial x_j}(\rho(\bar{u}_i\bar{u}_j+\bar{u}_iu_j'+u_i'\bar{u}_j+u_i'u_j'-\bar{C}\bar{u}_i\bar{u}_j-\bar{C}\bar{u}_iu_j'-\bar{C}u_i'\bar{u}_j-\bar{C}u_i'u_j' - C'\bar{u}_i\bar{u}_j-C'\bar{u}_iu_j'-C'u_i'\bar{u}_j-C'u_i'u_j'))$$

Average over time:

$$\frac{\partial}{\partial x_j}(\rho(\overline{\bar{u}_i\bar{u}_j}+\overline{\bar{u}_iu_j'}+\overline{u_i'\bar{u}_j}+\overline{u_i'u_j'}-\overline{\bar{C}\bar{u}_i\bar{u}_j}-\overline{\bar{C}\bar{u}_iu_j'}-\overline{\bar{C}u_i'\bar{u}_j}-\overline{\bar{C}u_i'u_j'} - \overline{C'\bar{u}_i\bar{u}_j}-\overline{C'\bar{u}_iu_j'}-\overline{C'u_i'\bar{u}_j}-\overline{C'u_i'u_j'}))$$

$$= \frac{\partial}{\partial x_j}(\rho(\bar{u}_i\bar{u}_j+\bar{u}_i\overline{u_j'}+\bar{u}_j\overline{u_i'}+\overline{u_i'u_j'}-\bar{C}\bar{u}_i\bar{u}_j-\bar{C}\bar{u}_i\overline{u_j'}-\bar{C}\bar{u}_j\overline{u_i'}-\bar{C}\overline{u_i'u_j'} - \bar{u}_i\bar{u}_j\overline{C'}-\bar{u}_i\overline{C'u_j'}-\bar{u}_j\overline{C'u_i'}-\overline{C'u_i'u_j'}))$$

$$= \frac{\partial \rho(\bar{u}_i\bar{u}_j+\overline{u_i'u_j'}-\bar{C}\bar{u}_i\bar{u}_j-\bar{C}\overline{u_i'u_j'}-\bar{u}_i\overline{C'u_j'}-\bar{u}_j\overline{C'u_i'}-\overline{C'u_i'u_j'})}{\partial x_j}$$

$$= \frac{\partial \rho(1-\bar{C})\bar{u}_i\bar{u}_j+\rho(1-\bar{C})\overline{u_i'u_j'}-\rho\bar{u}_i\overline{C'u_j'}-\rho\bar{u}_j\overline{C'u_i'}-\rho\overline{C'u_i'u_j'}}{\partial x_j}$$

$$\frac{\partial \rho(1-C)u_iu_j}{\partial x_j} = \frac{\partial \rho(1-\bar{C})\bar{u}_i\bar{u}_j+\rho(1-\bar{C})\overline{u_i'u_j'}-\rho\bar{u}_i\overline{C'u_j'}-\rho\bar{u}_j\overline{C'u_i'}-\rho\overline{C'u_i'u_j'}}{\partial x_j}$$

$$= \frac{\partial \rho(1-\bar{C})\bar{u}_i\bar{u}_j}{\partial x_j} - \frac{\partial(-\rho(1-\bar{C})\overline{u_i'u_j'}+\rho\bar{u}_i\overline{C'u_j'}+\rho\bar{u}_j\overline{C'u_i'}+\rho\overline{C'u_i'u_j'})}{\partial x_j}$$

If we leave out the averaging bars again on non-fluctuating quantities we get

$$\frac{\partial \rho(1-C)u_iu_j}{\partial x_j} - \frac{\partial(-\rho(1-C)\overline{u_i'u_j'}+\rho u_i\overline{C'u_j'}+\rho u_j\overline{C'u_i'}+\rho\overline{C'u_i'u_j'})}{\partial x_j}$$

We now define the convection related turbulent stress tensor τ^c_{ij}:

$$\tau^c_{ij} = -\rho(1-C)\overline{u'_i u'_j} + \rho u_i \overline{C' u'_j} + \rho u_j \overline{C' u'_i} + \rho \overline{C' u'_i u'_j}$$

The complete momentum balance is then:

$$\frac{\partial \rho(1-C)u_i}{\partial t} + \frac{\partial \rho(1-C)u_i u_j}{\partial x_j} = -\rho(1-C)g\delta_{i2} - (1-C)\frac{\partial p}{\partial x_i} + \frac{\partial \phi^a_i}{\partial t} + \frac{\partial \tau^c_{ij}}{\partial x_j} - f_i \tag{B.7}$$

Solid phase

The Reynolds averaged momentum balance for the solid phase can be derived equivalently.

$$\frac{\partial \rho_s C u_{s,i}}{\partial t} + \frac{\partial \rho_s C u_{s,i} u_{s,j}}{\partial x_j} = -C\frac{\partial p}{\partial x_i} - \rho_s C g \delta_{i2} + \frac{\partial T_{s,ij}}{\partial x_j} + f_i \tag{B.8}$$

Reynolds decomposition: $C = \bar{C} + C'$, $u_{s,i} = \bar{u_{s,i}} + u'_{s,i}$, $u_{s,j} = \bar{u}_{s,j} + u'_{s,j}$.

The first term:

$$\frac{\partial \rho_s C u_{s,i}}{\partial t} = \frac{\partial \rho \bar{C} \bar{u}_{s,i}}{\partial t} - \frac{\partial \rho_s \overline{C' u'_{s,i}}}{\partial t} \tag{B.9}$$

We will define the acceleration related turbulent flux $\phi^{s,a}_{s,i}$ as

$$\phi^{s,a}_{s,i} = \rho_s \overline{C' u'_{s,i}}$$

The second term:

$$\frac{\partial \rho_s C u_{s,i} u_{s,j}}{\partial x_j} = \frac{\partial \rho_s (\bar{C} + C')(\bar{u}_{s,i} + u'_{s,i})(\bar{u}_{s,j} + u'_{s,j})}{\partial x_j}$$

$$= \frac{\partial \rho_s(\bar{C}\bar{u}_{s,i} + \bar{C}u'_{s,i} + C'\bar{u}_{s,i} + C'u'_{s,i})(\bar{u}_{s,j} + u'_{s,j})}{\partial x_j}$$

$$= \frac{\partial}{\partial x_j}(\rho_s(\bar{C}\bar{u}_{s,i}\bar{u}_{s,j}+\bar{C}\bar{u}_{s,i}u'_{s,j}+\bar{C}u'_{s,i}\bar{u}_{s,j}+\bar{C}u'_{s,i}u'_{s,j}+C'\bar{u}_{s,i}\bar{u}_{s,j}+C'\bar{u}_{s,i}u'_{s,j}+C'u'_{s,i}\bar{u}_{s,j}+C'u'_{s,i}u'_{s,j}$$

Average over time:

$$\frac{\partial}{\partial x_j}(\rho_s(\overline{\bar{C}\bar{u}_{s,i}\bar{u}_{s,j}} + \overline{\bar{C}\bar{u}_{s,i}u'_{s,j}} + \overline{\bar{C}u'_{s,i}\bar{u}_{s,j}} + \overline{\bar{C}u'_{s,i}u'_{s,j}}$$
$$+\overline{C'\bar{u}_{s,i}\bar{u}_{s,j}} + \overline{C'\bar{u}_{s,i}u'_{s,j}} + \overline{C'u'_{s,i}\bar{u}_{s,j}} + \overline{C'u'_{s,i}u'_{s,j}}))$$

$$= \frac{\partial}{\partial x_j}(\rho_s(\bar{C}\bar{u}_{s,i}\bar{u}_{s,j} + \bar{C}\bar{u}_{s,i}\overline{u'_{s,j}} + \bar{C}\bar{u}_{s,j}\overline{u'_{s,i}} + \bar{C}\overline{u'_{s,i}u'_{s,j}}$$
$$+\bar{u}_{s,i}\bar{u}_{s,j}\overline{C'} + \bar{u}_{s,i}\overline{C'u'_{s,j}} + \bar{u}_{s,j}\overline{C'u'_{s,i}} + \overline{C'u'_{s,i}u'_{s,j}}))$$

$$= \frac{\partial \rho_s(\bar{C}\bar{u}_{s,i}\bar{u}_{s,j} + \bar{C}\overline{u'_{s,i}u'_{s,j}} + \bar{u}_{s,i}\overline{C'u'_{s,j}} + \bar{u}_{s,j}\overline{C'u'_{s,i}} + \overline{C'u'_{s,i}u'_{s,j}})}{\partial x_j}$$

$$= \frac{\partial(\rho_s\bar{C}\bar{u}_{s,i}\bar{u}_{s,j} + \rho_s\bar{C}\overline{u'_{s,i}u'_{s,j}} + \rho_s\bar{u}_{s,i}\overline{C'u'_{s,j}} + \rho_s\bar{u}_{s,j}\overline{C'u'_{s,i}} + \rho_s\overline{C'u'_{s,i}u'_{s,j}})}{\partial x_j}$$

$$\frac{\partial \rho_s C u_{s,i}u_{s,j}}{\partial x_j} = \frac{\partial(\rho_s\bar{C}\bar{u}_{s,i}\bar{u}_{s,j} + \rho_s\bar{C}\overline{u'_{s,i}u'_{s,j}} + \rho_s\bar{u}_{s,i}\overline{C'u'_{s,j}} + \rho_s\bar{u}_{s,j}\overline{C'u'_{s,i}} + \rho_s\overline{C'u'_{s,i}u'_{s,j}})}{\partial x_j}$$

$$= \frac{\partial \rho_s\bar{C}\bar{u}_{s,i}\bar{u}_{s,j}}{\partial x_j} + \frac{\partial(\rho_s\bar{C}\overline{u'_{s,i}u'_{s,j}} - \rho_s\bar{u}_{s,i}\overline{C'u'_{s,j}} + \rho_s\bar{u}_{s,j}\overline{C'u'_{s,i}} + \rho_s\overline{C'u'_{s,i}u'_{s,j}})}{\partial x_j}$$

If we leave out the averaging bars again on non-fluctuating quantities we get

$$\frac{\partial \rho_s C u_{s,i}u_{s,j}}{\partial x_j} + \frac{\partial(\rho_s C\overline{u'_{s,i}u'_{s,j}} - \rho_s u_{s,i}\overline{C'u'_{s,j}} - \rho_s u_{s,j}\overline{C'u'_{s,i}} - \rho_s\overline{C'u'_{s,i}u'_{s,j}})}{\partial x_j}$$

We now define the convection related turbulent stress tensor $\tau^{s,c}_{s,ij}$:

$$\tau^{s,c}_{s,ij} = \rho_s C\overline{u'_{s,i}u'_{s,j}} - \rho_s u_{s,i}\overline{C'u'_{s,j}} - \rho u_{s,j}\overline{C'u'_{s,i}} + \rho_s\overline{C'u'_{s,i}u'_{s,j}}$$

The complete momentum balance is then:

$$\frac{\partial \rho_s C u_{s,i}}{\partial t} + \frac{\partial \rho_s C u_{s,i} u_{s,j}}{\partial x_j} = -\rho_s C g \delta_{i2} - C \frac{\partial p}{\partial x_i} + \frac{\partial \tau_{s,i}^{s,a}}{\partial t} + \frac{\partial \tau_{s,ij}^{s,c}}{\partial x_j} + \frac{\partial T_{s,ij}}{\partial x_j} + f_i \quad \text{(B.10)}$$

Appendix C

Test case for fluid part of DPM

In this case the upper boundary flows with constant velocity, inducing a shearflow in the lower layers. Eventually a steady state is reached. The (steady state) case is sketched in figure C.1.

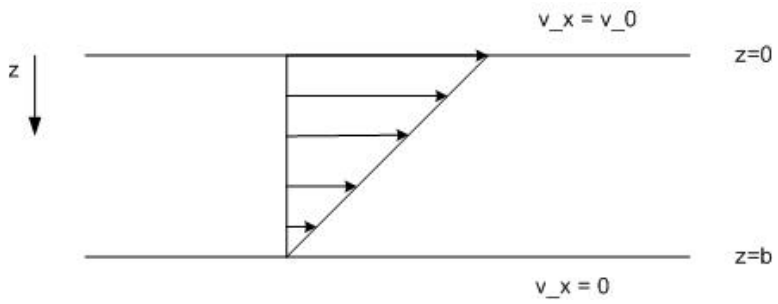

Figure C.1: Sketch of the shearflow case

C.0.3 Analytical solution

The analytical solution of this problem is described in detail in the book of Bird *et al.* [4]. A short summary of the solution strategy and the solution itself are given below.

As the velocities in the y and z direction, v_y and v_z, are zero, v_x does not change in the x and y-direction, and the pressure gradient in the x-direction is assumed to be zero, the momentum balance reduces to:

$$\frac{\partial v_x}{\partial t} = \nu \frac{\partial^2 v_x}{\partial z^2} \tag{C.1}$$

The following boundary and initial conditions apply:

$$\begin{aligned} v_x &= 0 \quad at \quad t = 0 \quad for\ all \quad 0 \leq z \leq b \\ v_x &= v_0 \quad at \quad z = 0 \quad for\ all \quad t \geq 0 \\ v_x &= 0 \quad at \quad z = b \quad for\ all \quad t \geq 0 \end{aligned}$$

The PDE is solved using the method of combination of variables. We therefore define the following dimensionless variables:

$$\phi = \frac{v_x}{v_0}; \quad \eta = \frac{z}{b}; \quad \tau = \frac{\nu t}{b^2}$$

The PDE then transforms to

$$\frac{\partial \phi}{\partial \tau} = \frac{\partial^2 \phi}{\partial \eta^2} \tag{C.2}$$

with the following boundary and initial conditions:

$$\phi = 0 \quad at \quad \tau = 0$$
$$\phi = 1 \quad at \quad \eta = 0$$
$$\phi = 0 \quad at \quad \eta = 1$$

We know that the solution must be a superposition of a steady state solution and a time dependant solution, where the latter must vanish for $t \to \infty$:

$$\phi(\eta, \tau) = \phi_\infty(\eta) - \phi_t(\eta, \tau)$$

It can easily be verified that the steady state solution ($\frac{\partial \phi}{\partial \tau} = 0$) is

$$\phi_\infty = 1 - \eta$$

Using the method of separation of variables the time dependent part of the solution can be found. The complete solution is then (n is an integer):

$$\phi(\eta, \tau) = (1 - \eta) - \sum_{n=1}^{\infty} (\frac{2}{n\pi}) exp(-n^2\pi^2\tau) sin(n\pi\eta) \tag{C.3}$$

C.0.4 Numerical implementation

The shearflow case was implemented in the DPM as follows. On the lower boundary a no slip boundary condition was imposed (flag number 3), on the upper boundary the pressure was prescribed (flag 5), while a constant velocity $v_x = v_0$ was imposed as well. On the front and back boundaries a free slip condition (flag 2) was imposed, and on the left and right hand side boundaries periodic boundary conditions are prescribed (flag 9). The flagmatrix is shown

in figure C.2.

Figure C.2: Flagmatrix showing the boundary conditions. Left: Cross section in x-z direction. Right: Cross section in x-y direction. Flag 1 is an interior cell.

A velocity of $v_x = 0.05m/s$ was chosen, in order to be sure that the flow in the simulation would remain laminar. The simulated domain was 0.02 m wide, 0.02 m high, and $1.2 * 10^{-3}$ m deep[1]. The grid has 50 flow cells in the x and z-direction, and 1 in the y-direction. The time step used was $1.0 * 10^{-4}$ s.

C.0.5 Comparison between analytical solution and simulation results and conclusion

Although no perfect overlap is found, the results of the simulation show rather good agreement with the analytical solution (figure C.3). The fluid part of the DPM thus seems to give accurate and realistic results.

[1] 6 times the typical diameter of sand particles we eventually want to simulate.

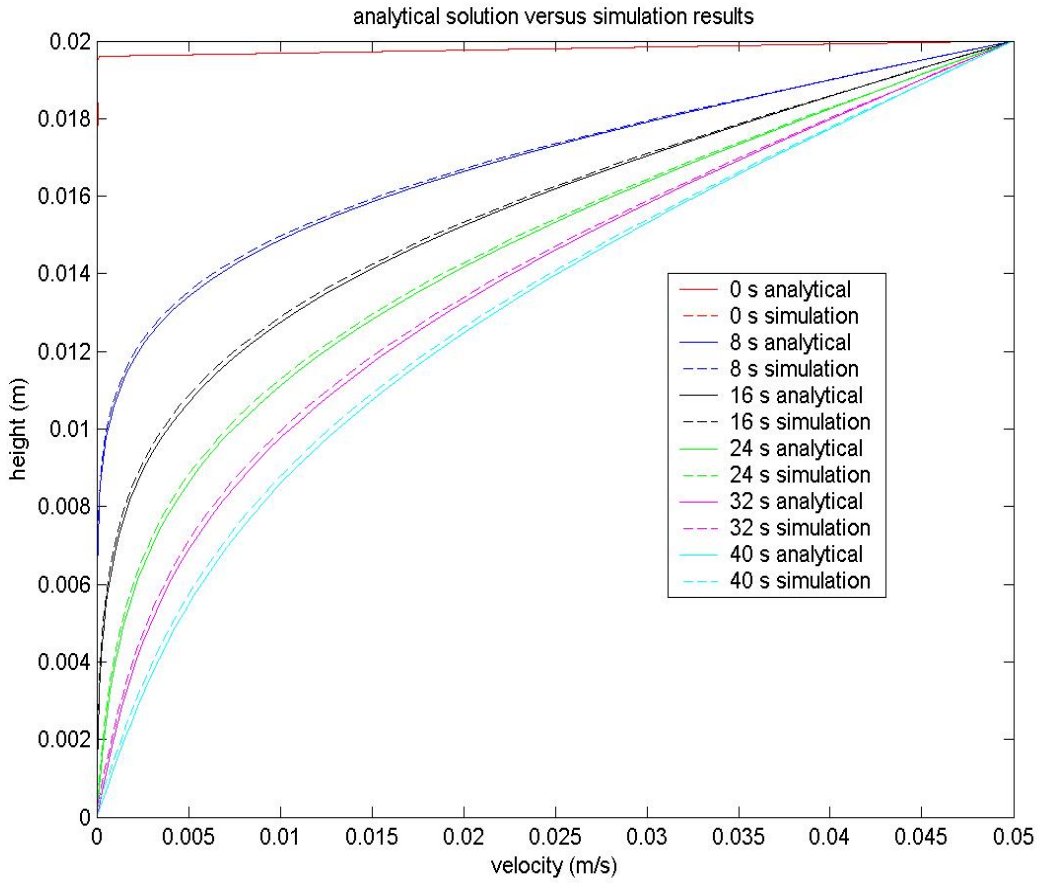

Figure C.3: Comparison of the analytical solution (solid lines) and the simulation results (striped lines)